THE ASTROPHYSICAL JOURNAL, 542:428–445, 2000 October 10

HUBBLE SPACE TELESCOPE OBSERVATIONS OF THE LUMINOUS BLUE VARIABLE/W-R ECLIPSING BINARY SYSTEM HD 5980[1]

GLORIA KOENIGSBERGER AND LEONID GEORGIEV
Instituto de Astronomía, UNAM, Apdo. Postal 70-264, Mexico D.F. 04510, Mexico
RODOLFO BARBÁ[2]
Facultad de Ciencias Astronómicas y Geofísicas, Universidad Nacional de la Plata, Paseo del Bosque S/N, B19000FWA La Plata, Argentina
ZLATAN TZVETANOV
Johns Hopkins University, Baltimore, MD
NOLAN R. WALBORN
Space Telescope Science Institute, Baltimore, MD
VIRPI S. NIEMELA[3] AND NIDIA MORRELL[2]
Facultad de Ciencias Astronómicas y Geofísicas, Universidad Nacional de la Plata, Paseo del Bosque S/N, B19000FWA La Plata, Argentina
AND
REGINA SCHULTE-LADBECK
University of Pittsburgh, Pittsburgh, PA
Received 2000 March 12; accepted 2000 May 11

ABSTRACT

We report the results of *Hubble Space Telescope* STIS observations of the intriguing luminous blue variable/Wolf-Rayet binary system HD 5980 in the Small Magellanic Cloud. Although its spectral characteristics (WN6) are currently very similar to those observed in 1995 in the FUV, some of the line fluxes continue with the increasing trend observed since the 1980s. The erupting star still dominates the emission-line spectrum, and a radial velocity curve from UV lines is derived, supporting previous estimates of its mass (50 $M_\odot$). A rough estimate of 2×10^{-4} $M_\odot$ yr^{-1} for the current mass-loss rate of this star is derived. The only spectral lines attributable to the close companion are the very extended P Cygni absorption components of the strong UV lines, present only during the eclipse of the eruptor, implying that the wind-wind collision shock cone winds tightly around this companion. A third stellar component contributing to the spectrum is detected through the presence of stationary photospheric absorption lines in the UV spectrum. This object contributes ~30% to the UV continuum luminosity. A new set of ISM absorption components at −680 km s^{-1} has appeared as a result of the shock interface between the slow wind (~400 km s^{-1}) that emerged during the 1994 eruption and the subsequently emerging fast wind (~2000 km s^{-1}) phases.

Subject headings: binaries: general — stars: evolution — stars: individual (HD 5980) — stars: variables: other — stars: winds, outflows — stars: Wolf-Rayet

1. INTRODUCTION

Over the past few years considerable progress has been made in the development of theoretical models of massive stars extending from the main sequence to the supernova explosion. The theoretical evolutionary tracks provided by these models are used in studies of a wide range of topics, including chemical enrichment of the ISM, galaxy evolution, and the age and evolution of starburst regions in extragalactic objects. A very important evolutionary stage, from the standpoint of the formation of ISM structures and chemical enrichment, is that of the Wolf-Rayet (W-R) stars, and the spectra of many active extragalactic objects display emission lines that are typical of these stars. Because of the short lifetime of the W-R phase (~10^5 yr), the presence of W-R stars in a starburst region can potentially provide a strong constraint on the age of the starburst (see Leitherer 1999).

The W-R stars are characterized by extremely broad and strong emission lines that are formed in their rapidly (2000–3000 km s^{-1}) expanding stellar winds (see, for example, the recent reviews by Willis 1999). Historically, Population I W-R stars have been understood as direct descendents of massive O-type stars that have already left the main sequence (MS) and are on their way to the final stages of stellar evolution prior to the supernova explosion. As they leave the MS, the H-rich layers of their atmospheres that have not already been removed by the stellar winds are believed to be violently ejected during what is known as the luminous blue variable (LBV) phase of its evolution (see Maeder 1997 and references therein). The detailed physical processes by which these ejections take place are still a matter of debate (Stothers & Chin 1996; Langer et al. 1994; García-Segura et al. 1996). A number of LBVs have been observed through various phases of their activity (comprehensive reviews are given by Humphreys & Davidson 1994 and Bohannan 1997), and the list of LBVs includes such illustrious members as η Carinae, P Cygni, and R127. The "major" eruptions that have occurred in some of these

[1] Based on observations with NASA/ESA *Hubble Space Telescope* obtained at the Space Telescope Science Institute which is operated by the Association of Universities for Research in Astronomy, Inc., under NASA Contract NAS 5-26555.
[2] Member of Carrera del Investigador, CONICET, Argentina.
[3] Member of Carrera del Investigador, CIC, Prov. Buenos Aires, Argentina

objects begin to approach supernovae in terms of luminosities and ejected masses (Gallagher 1997).

Under the assumption that all Population I W-R stars represent evolutionary stages that appear after massive stars have left the MS, their presence in a starburst region would seem to provide a precise lower limit to the age of the burst. However, there are indications that W-R-star spectral characteristics may also be associated with very young and massive stars: recent analysis of the most luminous W-R stars in R136a (de Koter, Heap, & Hubeny 1997), the tight cluster of massive stars in 30 Doradus in the LMC, indicates that these stars still lie on the MS, and have theoretical masses in excess of 120 $M_{\odot}$. A similar conclusion for three W-R stars in the Galactic cluster NGC 3603 is reached by Crowther & Dessart (1998) and by Schmutz & Drissen (1999), with these stars having ages less than 2 Myr. The W-R-like emission lines seem to be present simply because of the very large mass-loss rates present in these young stars (Heap 1999). This result, if confirmed, would imply that W-R features in starburst spectra are indicative either of an extremely recent event of star formation (<2 Myr), or ongoing star formation, as well as one old enough for post-MS W-R stars to be present.

Furthermore, studies of the effects that close binary stars may produce in the evolution of stellar populations are starting to suggest that the role of binary stars cannot be neglected when deducing the properties of starburst regions from population synthesis models (Van Bever et al. 1998; Dionne 1999). For example, Mas-Hesse & Cerviño (1999) find that due to mass transfer in the binary systems, the duration of the formation period of W-R stars can be extended to 15 Myr. These results, however, depend on the interaction effects assumed to take place in the binary system as it evolves. In this context, a detailed study of an extragalactic binary system that may be going through the LBV transition into the W-R phase is very relevant.

The LBV/W-R eclipsing binary ($P = 19.266$ days) HD 5980 is located in the periphery of NGC 346, which is the largest H II region of the Small Magellanic Cloud (SMC) and contains over half of the known O stars in that galaxy (Massey, Parker, & Garmany 1989). Prior to 1980, it was classified as WN+OB: (Breysacher, Moffat, & Niemela 1982 and references therein). This classification was based on the spectral appearance. However, there is controversy regarding whether a reliable velocity has ever been determined for the OB component. The absorption-line orbit by Breysacher et al. (1982) relies on only two deviating data points, and, as noted by these authors, the radial velocities of the He II 4686 emission probably do not reflect the true orbital motion of the WN star either.

A further radial velocity study of HD 5980 based on data obtained during 1980–1983 (Niemela 1988; Niemela et al. 1997) showed large amplitude antiphased radial velocity variations of the emission lines of N V 4603 and N IV 4058, suggesting that two emission-line stars form the system. The derived spectral classification was WN3+WN4, with the WN3 star (possessing N V 4603 emission) eclipsing the companion at phase 0.0. Radial velocities of He I 4471 and H9 absorption lines could not be shown to belong to either of the binary components, possibly being associated with an intervening line-of-sight OB star (a third component, whose existence we confirm below).

By 1992 the presence of N III 4640 led to a classification as WN6 (Koenigsberger et al. [1994]), and its radial velocity curve was the same as that of N V 4603 in 1980–1983, indicating that the same star had changed the ionization state of its wind. By this time, no spectral signature of the companion star could be detected. In fact, the only clear spectral signature of this companion star ever seen is the N IV 4058 emission line, but in the 1988–1992 data, this line no longer follows the orbital motion of either of the two stars. In addition, the photospheric absorption lines attributable to a possible OB star were no longer observed.

In 1994 HD 5980 underwent an LBV-type eruptive event at which time its spectral type was at least as cool as a WN11 star (Heydari-Malayeri et al. 1997, using the extended WN classification introduced by Smith, Shara, & Moffat 1994). The transition through the WN3–WN11 spectral sequence developed by HD 5980 during the past 20 years before and during the eruption reflects systematically decreasing effective temperatures of the stellar wind in the range 90,000 to 20,000 K (adopting result for other stars of Hamann & Koesterke [1998] and Crowther & Smith [1996]).

The two stars in the 19.3 per day orbit were labeled by Barbá et al. (1996) as star A and star B, a nomenclature that we will follow throughout this paper. Star A is eclipsed at phase 0.36 and star B is eclipsed at phase 0.00. Star A is the star whose wind structure has been undergoing strong changes (Barbá et al. 1996; Koenigsberger et al. 1998a; Moffat et al. 1998). Between the years 1978 and 1991, it systematically reduced its wind velocity and its degree of ionization (Koenigsberger 1994, 1998a) while becoming brighter at visual wavelengths. In 1993 it presented a precursor outburst, followed in 1994 by a major LBV-type eruption with a visual magnitude enhancement of ~ 3.8 mag (Barbá et al. 1995; Bateson & Jones, 1994). At this stage, the visual spectrum was transformed from a WN type to one nearly identical to certain phases of the Galactic LBV AG Car (Barbá et al. 1995).

Monitoring of the eruption at ultraviolet wavelengths with the *International Ultraviolet Explorer* (*IUE*; Boggess et al. 1978a, 1978b) started approximately 4 months after maximum light had been achieved, at which time the UV ($\lambda\lambda$1200–2000) spectrum had a strong resemblance to that of a B1.5Ia^{+} star (Koenigsberger et al. 1996). There are unfortunately no spectra available of the system during maximum, so it could have achieved even later spectral types than B1.5. The radius of the erupting star was estimated by Koenigsberger et al. (1998a) to be over 100 $R_{\odot}$ (i.e., at least as large as the orbital separation) with its spectrum still completely dominating the light emerging from the system. By this time, the LBV-eruption light curve was on its declining branch, and an increase in the degree of ionization in the wind was observed and followed until the spectrum reverted to a WN6 type (Barbá, Niemela, & Morrell 1997) one year after maximum. The wind velocities also reverted to their pre-eruption values (Koenigsberger et al. 1998a).

A non-LTE stellar wind model was fitted to optical and UV spectra obtained on 1994 December 30–31, at a time when wind velocities were increasing rapidly. From this model, the hydrogen abundance [N(He)/N(H) = 0.43 by number], the mass-loss rate ($\dot{M} \sim 10^{-3}\ M_{\odot}\ \mathrm{yr}^{-1}$), effective temperature ($T_{\mathrm{eff}} = 35500$ K), luminosity ($L_{\mathrm{eruptor}} = 3 \times 10^{6}\ L_{\odot}$), and stellar radius ($R_{*} = 48\ R_{\odot}$) were estimated (Koenigsberger et al. 1998b). These parameters correspond to star A, and were derived under the assumptions inherent

to the *standard model* (see discussions by Hillier 1995 and Schmutz 1995). These parameters place star A on the H-R Diagram near the evolutionary tracks for a 120 $M_\odot$ ZAMS object.

The number of stars constituting HD 5980 has been an issue of discussion since Massey, Parker, & Garmany (1989) saw indications of a second point source on their photographic image data and Breysacher & Perrier (1991) presented a solution for the eclipse light curve suggesting the presence of a third object in HD 5980. According to this calculation, the "third light" contribution amounts to close to 30% of the total optical light of the system. However, HD 5980 appeared as a point source on a *Hubble Space Telescope* (*HST*) image obtained with the WFPC2 in 1994 May (proposal 5394, data set U29T0101T, F255W; PI D. Welty), precluding the presence of a third object less than 3 mag fainter than HD 5980, at angular distances on the order of 0.″1, consistent with the finding of Heydari-Malayeri et al. (1997) from subarcsecond adaptive optics observations.

Other problems of interest that can be addressed with HD 5980 include the influence of its wind on the surrounding ISM environment. The winds in 1978–1981 had velocities over 3000 km s^{-1}, while one of the characteristics of the 1994 eruption is the very slow wind velocities (200–800 km s^{-1}), which were followed by a rapid increase up to values of 2000 km s^{-1} within approximately 6 months (Koenigsberger et al. 1998a). The rapidly outflowing wind is expected to plow into the slower wind, producing a shock discontinuity that should eventually be observed as a circumstellar shell, perhaps such as is now observed in Eta Carinae (García-Segura et al. 1996). Hence, we may be witnessing the early stages of the formation of circumstellar structure such as the Homunculus. Finally, HD 5980 also presents a magnificent challenge for the study of wind-wind collision effects (Moffat et al. 1998 and references therein), owing to its eccentric orbit and the variations in the wind velocity of one of the stars, over long timescales.

In this paper we present the results obtained from the analysis of five *HST* observations of HD 5980, which will allow us to address some of the problems stated above.

2. OBSERVATIONS AND DATA ANALYSIS

The observations were carried out with the *Hubble Space Telescope* in five visits, during 1999 May 6–17, using the Space Telescope Imaging Spectrograph (STIS; Kimble et al. 1998). Each visit consisted of two orbits, using the MAMA detector for observations in high-dispersion mode in the UV range in one orbit, and the CCD detector for observations in low-dispersion mode in the near UV, optical and near IR range. The complete wavelength coverage for observations in each visit is $\lambda\lambda$1150–10260, with wavelength resolutions ranging from $\sim$0.02 Å in the far UV ($\lambda\lambda$1150–1710, MAMA detector) to $\sim$5 Å pixel^{-1} in the $\lambda\lambda$7000–10260 region. Table 1 lists the instrument configurations used. Table 2 gives the dates and binary orbital phases for each *HST* visit to HD 5980. The phases were computed with the ephemeris of Sterken & Breysacher (1997), $P = 19.2654$ days, $T_0 = 2443158.705$.

The *HST* observations are complemented with data obtained between 1989–1995 with the *IUE* (see Koenigsberger et al. 1994 and 1998a for descriptions of these data sets) and *HST* archival data of stars in NGC 346.

The orbital phases of the observations were selected to occur at the two eclipses ($\phi = 0.00$,0.36), near periastron passage ($\phi = 0.05$), near the expected maximum radial velocity values ($\phi = 0.83$,0.15) of the eccentric orbit, and at phase $\phi = 0.40$ (wind eclipse). Phases 0.83 and 0.40 are in common with most of the sets of *IUE* data obtained since 1986 and allow a reliable comparison of epoch-dependent changes in the spectrum from this time onward. Unfortunately, because of spacecraft problems, the observation at $\phi = 0.00$ was not performed. In Figure 1 we present a schematic illustration of the orbit of star A, based on the orbital solution of Breysacher & Perrier (1991), upon which we indicate the times of the *HST* observations.

The data were reduced through the STIS standard pipeline at STScI (for details about the procedure see Voit 1997, chap. 21). The echelle orders of the far UV data were merged using MIDAS.[4] Measurements of equivalent widths and fluxes in the lines were made with IRAF[5] by integration over the wavelength range defined by the feature. As is generally the case for W-R-type spectra, the largest uncertainty arises from the difficulty in placing the continuum level, particularly in the far UV range below 1500 Å due to the presence of the very large number of overlapping lines. For each spectrum, the continuum level was chosen by visual interpolation, and an error estimate was made by obtaining measurements using two extreme locations of the continuum level. We estimate the uncertainty in the equivalent-width measurements to be $\sim$10%.

Two additional problems for measuring emission lines are the line blending due to closely spaced lines and the presence of superimposed interstellar and photospheric absorption lines. The spectra of HD 5980 contain multiple ISM components, corresponding to the Galaxy ($v = 0$ km s^{-1}), the SMC ($v = +150$ km s^{-1}), and a third system at $+300$ km s^{-1} of unknown origin (de Boer & Savage 1980). Before the integration over emission-line profiles was per-

[4] MIDAS is the Munich Image Data Analysis System developed by ESO.

[5] IRAF, was developed by the National Optical Astronomy Observatories.

TABLE 1

HST/STIS OBSERVATIONS

Detector	Spectral Region (Å)	Scale (Å pixel^{-1})	Grating	Slit (arcsec)	Exposure Time (s)
MAMA.....	1150–1698	0.01–0.02	E140M	0.2 × 0.2	3236
CCD.....	1677–3070	1.35	G230LB	52 × 0.2	240
CCD.....	2920–5694	2.73	G430L	52 × 0.2	60
CCD.....	5292–10260	4.92	G750L	52 × 0.2	72
CCD.....	5452–6018	0.56	G750M	52 × 0.2	120
CCD.....	6484–7050	0.56	G750M	52 × 0.2	210

TABLE 2

HST Observation Dates and Phases

Visit	Observation Number	Region (Å)	Date (1999 May)	HJD (2,450,000.+)	Orbital Phase
1.....	o550o1010	1677–3070	6	1304.771	0.83
	o550o1020	2920–5694			
	o550o1030	5452–6018			
	o550o1040	6484–7050			
	o550o1050	5292–10260			
	o550o1070	1150–1698			
3.....	o550o3010	1677–3070	10	1308.896	0.05
	o550o3020	2920–5694			
	o550o3030	5452–6018			
	o550o3040	6484–7050			
	o550o3050	5292–10260			
	o550o3070	1150–1698			
4.....	o550o4010	1677–3070	12	1310.833	0.15
	o550o4020	2920–5694			
	o550o4030	5452–6018			
	o550o4040	6484–7050			
	o550o4050	5292–10260			
	o550o4070	1150–1698			
5.....	o550o5010	1677–3070	16	1314.905	0.36
	o550o5020	2920–5694			
	o550o5030	5452–6018			
	o550o5040	6484–7050			
	o550o5050	5292–10260			
	o550o5070	1150–1698			
6.....	o550o6010	1677–3070	17	1315.843	0.41
	o550o6020	2920–5694			
	o550o6030	5452–6018			
	o550o6040	6484–7050			
	o550o6050	5292–10260			
	o550o6070	1150–1698			

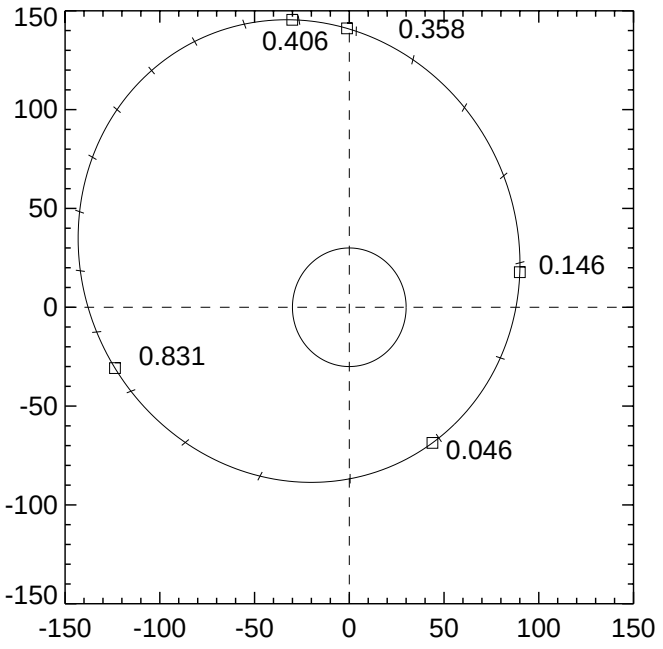

FIG. 1.—Schematic representation of the orbit of star A, indicating the phases at which the *HST* spectra were obtained. This drawing was made using the following parameters: $P = 19.266$ days, $e = 0.31$, $i = 88°$, $\omega_A = 133°$, $\omega_B = 313°$, and $a = 120\ R_\odot$. The superposed tick marks on the orbit are separated in orbital phase by $\delta\phi = 0.05$, and the open squares indicate the times at which our *HST* observations were obtained. The x- and y-axes are in units of solar radii.

formed, these superposed absorption lines were "cut out" in the high-dispersion data.This procedure, however, is not possible in lower resolution spectra. We estimate that the neglect of the effect due to ISM lines leads to an *underestimate* of the emission-line equivalent widths and fluxes that can be as large as 15%. It is important to keep this effect in mind, particularly when dealing with low-resolution spectra of very distant objects, where multiple ISM components will most certainly be present. In the case of overlapping lines, the strengths that were measured correspond to that portion of the line which could be separated from the adjacent line.

The results obtained from these measurements are presented in Table 3, where they are listed as follows: in column (1), a reference wavelength that corresponds to the central wavelength of the feature in spectra observed during the first visit to HD 5980 ($\phi = 0.83$); in column (2), the identification of the dominant ionic species; in columns (3)–(7), the equivalent width measured on each of the five sets of spectra; and in columns (8)–(12), the corresponding nondereddened flux values. Positive (negative) values of EW indicate absorption (emission) features. The P Cyg absorption components are noted by "a" in column (2), and a colon is used to denote uncertain values.

The position of the lines was measured with IRAF, either by fitting a Gaussian profile to spectral features where such a function is a good approximation, or by computing the midpoint between two continuum locations enclosing the line. When appropriate, overlapping lines were deblended

TABLE 3

MEASUREMENTES OF EMISSION AND P CYG ABSORPTIONS

		EW (Å)					FLUX (10^{-13} ergs cm^{-2}s^{-1} Å^{-1})				
λ_{ref} (1)	ION (2)	0.83 (3)	0.05 (4)	0.15 (5)	0.36 (6)	0.40 (7)	0.83 (8)	0.05 (9)	0.15 (10)	0.36 (11)	0.40 (12)
1235.2.....	N va	9.6	8.9	9.5	11.0	9.9	−396.	−313.	−431.	−410.	−388.
1245.5.....	N v+C iii	−9.7	−8.5	−9.4	−5.5	−4.8	404.	298.	425.	204.	185.
1254.4.....	Fe vi	−1.5	−1.5	−1.5	−0.9	−1.4	64.9	53.7	69.3	32.8	52.7
1267.0.....	Fe vi	−0.7	−1.2	0.7	−0.3	−0.7	31.2	40.0	31.2	10.2	28.0
1273.3.....	Fe vi, N iv	−0.7	−0.8	−0.7	−0.3	−0.6	29.3	27.2	31.4	9.8	25.3
1279.8.....	Fe vi	−0.8	−1.1	−0.6	−0.4	−1.0	34.0	37.0	29.4	13.7	38.9
1288.0.....	Fe vi, N iv	−1.3	−1.4	−1.2	−1.0	−1.5	53.4	48.3	54.0	36.4	57.7
1291.7.....	Fe vi, N iv	−0.5	−0.6	−0.3	np	−0.4	19.4	20.5	12.9	np	14.4
1297.2.....	Fe vi, N iv	−0.7	−0.9	−0.8	−0.4	−0.9	29.8	31.6	35.3	15.3	36.1
1311.2.....	Fe vi, N iv	−1.2	−1.5	−0.8	−1.0	1.4	48.1	50.9	36.1	38.7	58.4
1323.0.....	Fe v, N iv, Ni V:	−1.7	−1.6	−1.0	−1.8	−1.9	69.8	57.5	46.3	69.3	76.9
1331.5.....	Fe v, N iv	−1.1	−1.0	−0.4	−0.6	−0.8	43.9	35.2	12.6	21.4	31.2
1358.8.....	Fe va	1.5	1.1	1.1	0.2	0.2	−60.6	−39.0	−50.2	−8.3	−8.7
1364.7.....	Fe v	−1.3	−1.4	−0.6	−1.2	−1.2	54.1	49.1	26.1	42.3	46.5
1370.9.....	Fe va, O va	2.4	2.1	1.9	1.3	1.4	−97.9	−73.4	−86.1	−47.9	−55.1
1378.7.....	Fe v	−1.9	−2.0	−1.5	−2.6	−2.5	80.0	68.3	70.5	98.6	99.2
1389.4.....	Si iva	1.9	2.1	2.1	0.5	0.4	−78.5	−73.1	−94.7	−18.7	−17.2
1394.3.....	Si iv	−0.8	−0.7	−0.5	−1.2	−1.0	33.2	25.2	24.3	45.1	38.8
1398.6.....	Fe v:a	1.3	2.5	2.5	0.1	0.2	−53.7	−86.8	−114.0	−4.0	−7.5
1403.8.....	Si iva	1.5	bl	bl	...	0.5	−63.7	bl	bl	—	−18.3
1409.2.....	Si iv, O iv]	−1.3	−1.3	−1.0	−2.7	−2.3	52.4	46.0	45.1	102.6	91.7
1420.8.....	Fe v	−1.0	−1.0	−0.5	−1.0	−1.1	42.5	−34.7	23.8	38.4	42.0
1426.5.....	Fe v, C iiia	1.7	1.5	1.4	0.9	0.8	−69.7	−53.5	−65.8	−34.8	−33.2
1431.6.....	Fe v, C iii	−0.9	−0.9	−0.5	−0.5	−0.6	36.0	31.3	23.9	19.9	23.2
1436.8.....	Fe va, N iv	1.5	1.3	1.3	0.6	0.5	−61.6	−46.5	−58.8	−22.2	−21.0
1440.7.....	Fe v, N iv	−0.1	−0.04	−0.1	0.0	0.1	4.9	1.5	3.0	0.0	3.4
1444.4.....	Fe v, N iva	1.1	0.8	0.8	0.0	0.0	−45.5	−29.3	−35.4	0.0	0.0
1448.3.....	Fe v, N iv	−0.1	−0.1	—	−0.1	−0.1	3.8	2.9	—	2.8	3.6
1451.6.....	Fe va	1.1	1.0	1.1	0.0	0.0	−45.5	−29.3	−35.4	0.0	0.0
1456.0.....	Fe v:, Ti iv :a	0.9	0.6	0.5	0.2	em?	−38.4	−20.8	−20.9	−6.7	—
1461.1.....	Fe va	0.8	0.3:	0.6	0.0	0.0	−32.9	−11.1:	−28.7	0.0	−0.5
1475.5.....	N iv]a:	0.3	0.3	0.2	0.05	0.1	−11.3	−11.9	−7.9	−1.8	−4.4
1486.7.....	N iv]	−4.2	−5.2	−4.4	−5.1	−5.6	168.0	175.9	182.7	181.9	208.0
1498.8.....	Ni V:, N v:a	0.5	0.5	0.3	0.1	0.2	−19.2	−16.9	−12.0	−2.5	−6.2
1503.5.....	Ni V:, N v	−0.5	−0.4	−0.6	−0.4	−0.5	19.0	13.3	24.9	12.5	18.2
1542.9.....	C iva	10.5	10.2	10.5	11.0	10.4	−373.	−306.	−377.	−315.	−337.
1554.1.....	C iv	− 9.3	− 9.4	−10.2	−11.2	− 8.7	329.	289.	363.	318.	274.
1634.0.....	He iia	1.6	2.0	1.2	3.2	3.0	−49.1	−54.9	−37.0	−85.9	−84.7
1642.0.....	He ii	−44.1	−39.3	−40.9	−36.9	−34.5	1342.	1085.	1260.	973.	1004.
1712.7.....	N iva	2.5	2.5	2.0	2.3	2.6	−62.4	−45.5	−50.0	−42.5	−53.9
1722.5.....	N iv	−6.5	− 4.0	− 6.6	−3.1	−1.7	155.2	76.0	160.0	58.8	35.9
1736.1.....	Si iii	−0.3	−0.5	−0.7	−1.3	−0.7	8.4	7.5	17.2	23.9	13.9
1747.2.....	N iii	−0.3	−0.4	−0.3	−0.5	−0.4	6.7	6.8	8.5	9.4	7.2
1856.2.....	Al iii (ism)	0.3	0.3	0.3	0.3	0.3	−6.4	−5.3	−5.9	−4.8	−6.1
1864.9.....	Al iii (ism)	0.1	0.1	0.1	0.2	0.2	−2.8	−2.2	−2.2	−2.9	−3.3
1977.3.....	Fe iii:	−0.4	−0.2	−0.3	−0.4	−0.3	6.9	2.5	6.6	5.8	5.2
1993.4.....	Fe iii	−0.5	−0.4	−0.6	−0.6	−0.7	8.5	5.5	11.3	8.3	11.3
2027.8.....	Zn ii (ism)	0.3	0.3	0.3	0.3	0.3	−6.0	−4.5	−4.4	−4.3	−4.6
2149.8.....	Fe iii:, N iii	−1.0	−0.6	−0.8	−1.2	−1.2	13.8	8.8	11.0	13.2	15.2
2168.0.....	Fe iii	−0.5	−0.4	−0.5	−0.5	−0.6	7.3	4.8	7.5	5.3	6.9
2190.5.....	N iii	−1.0	−0.7	−0.8	−1.0	−0.9	13.3	7.6	11.5	10.7	10.7
2218.9.....	Ne iii:, Fe ii:	−1.2	−0.9	−1.3	−1.4	−1.0	16.3	9.8	17.9	14.2	11.8
2256.0.....	Ne iv:, Fe ii :	−1.5	−1.0	−1.3	−1.6	−1.2	19.0	10.4	16.5	16.5	13.1
2299.8.....	C iiia	0.3	0.1	0.1	0.2	0.1	−3.2	−1.3	−1.9	−1.6	−1.4
2310.9.....	C iii	−2.2	−1.9	−2.3	−2.9	−2.5	27.8	19.6	28.7	27.3	26.6
2392.5.....	He ii	−2.8	−2.3	−2.4	−3.1	−2.6	31.5	22.2	27.4	27.8	25.8
2515.4.....	He ii	−5.9	−4.3	−5.2	−5.8	−4.9	58.4	36.8	53.2	46.6	43.3
2737.3.....	He ii	−9.9	−8.0	−9.8	−10.8	−9.0	79.1	56.5	80.5	70.2	65.4
3207.7.....	He ii	−22.6	−21.6	−23.3	−28.1	−25.3	137.0	114.7	143.0	136.4	134.5
3362.1.....	N iii:	−1.6	−1.4	−1.3	−1.3	−0.9	8.2	6.3	7.0	5.5	4.1
3487.2.....	N iv	−6.1	−3.3	−5.9	−5.3	−5.4	29.6	13.4	29.2	20.6	23.0

TABLE 3—*Continued*

		EW (Å)					Flux (10^{-13} ergs cm^{-2}s^{-1} Å^{-1})				
λ_{ref} (1)	Ion (2)	0.83 (3)	0.05 (4)	0.15 (5)	0.36 (6)	0.40 (7)	0.83 (8)	0.05 (9)	0.15 (10)	0.36 (11)	0.40 (12)
3876.6.....	He Ia	0.5	0.4	0.3	0.3	0.4	−1.9	−1.4	−1.3	−0.7	−1.4
3895.2.....	He I	−3.7	−5.2	−3.4	−5.5	−4.8	13.2	15.5	13.0	15.6	15.1
3938.4.....	Ca II(ism)	0.3	0.2	0.2	0.2	0.2	−1.1	−0.9	−0.8	−0.5	−0.6
3974.5.....	H_ϵ+He I	−1.8	−1.9	−1.8	−2.3	−1.6	6.0	5.3	6.0	6.2	4.7
4031.7.....	He I	−1.9	−1.8	−2.0	−2.4	−2.0	6.0	5.0	6.7	6.3	5.7
4059.8.....	N IV	−4.1	−3.8	−4.0	−3.5	−3.9	13.3	10.4	13.1	9.0	11.0
4104.4.....	H_δ+N III+He II	−9.5	−9.7	−9.4	−11.1	−9.0	29.4	25.4	29.5	27.5	24.6
4204.5.....	He II	−4.4	−3.7	−3.7	−4.9	−4.0	12.3	8.8	10.5	11.0	9.9
4345.3.....	H_γ+He II	−7.9	−8.3	−8.0	− 9.4	−8.1	20.3	17.8	20.8	19.7	18.1
4460.4.....	He Ia	0.4	0.6	0.1	0.1	0.2	−1.0	−1.3	−0.2	−0.2	−0.4
4478.0.....	He I	−1.3	−2.2	−1.3	−2.7	−2.0	3.2	4.3	3.2	5.0	4.2
4520.4.....	N III	−1.4	−1.9	−2.3:	−2.4	−1.3	3.2	3.6	5.5:	4.3	2.6
4547.2.....	He II	−6.7	−6.2	−5.2	−7.9	−6.2	15.2	11.8	12.2	14.4	12.5
4611.2.....	N V	−0.4	−0.1	−0.3	−0.3	−0.2	1.0	0.3	0.7	0.5	0.4
4643.9.....	N III	−8.7	−8.6	−6.5	−8.1	−6.3	17.9	15.4	14.3	13.9	11.9
4692.2.....	He II	−111.5	−100.8	−103.6	−118.	−116.	220.	170.	216.	203.	209.
4868.4.....	H_β+He II	−19.8	−20.6	−17.9	−23.4	−20.8	36.3	31.2	34.2	35.0	33.5
4926.0.....	He I	−3.2	−3.7	−2.3	−3.7	−2.5	5.7	5.5	4.3	5.4	3.9
5025.3.....	He I	−0.8	−1.8	−1.6	−1.4	−1.5	1.4	2.5	2.7	1.9	2.0
5418.5.....	He II	−17.9	−16.3	17.1	−21.9	−17.9	24.2	18.5	24.0	24.4	21.4
5807.8.....	C IV	−6.4	−5.5	−6.2	−7.4	−8.6	6.6	4.8	6.5	6.2	7.6
5858.7.....	He Ia	1.3	0.6	0.1	0.5	0.6	−1.3	−0.5	−0.1	−0.4	−0.5
5884.3.....	He I	−11.4	−12.7	−11.7	−15.7	−14.0	11.3	10.7	11.8	12.7	12.0
6568.2.....	H_α+He II	−70.4	−69.5	−74.3	−89.0	−79.9	50.1	41.3	53.5	52.4	50.5
6686.1.....	He I+He II	−13.1	−13.0	−11.3	−15.3	−11.7	8.7	7.4	7.8	8.5	7.0
6896.9.....	He I	−6.1	−4.0	−5.7	−6.0	−5.1	3.7	2.1	3.6	3.0	2.8
7602.3.....	He II+N IV	−12.4	−11.4	−11.3	−13.8	−13.2	6.2	4.8	5.7	5.6	5.8
8247.5.....	He II	−20.0	−15.9	−21.1	−23.0	−19.8	7.9	5.4	8.3	7.2	6.9
9357.0.....	He II	−37.6	−37.5	−38.4	−44.6	−43.8	9.5	8.2	9.7	9.3	9.8

NOTE.—Positive (negative) values of EW indicate absorption (emission) features. The P Cyg absorption components are noted by "a" in column (2), and a colon is used to denote uncertain values.

by fitting multiple Gaussians. The radial velocities of lines in the archival *IUE* data were measured in the same manner as the *HST* data. Most of the strong emission-line profiles on the high-resolution spectra are distorted by their P Cygni absorption components, by the presence of superimposed absorption features, and by variable effects due to the interaction of the two stars in the binary system. Hence, in general, a Gaussian distribution is a very poor approximation to the actual line profile.

Spectral lines were identified with the lists given by Striganov & Svetitskii (1968), Kelly & Palumbo (1973), Bruhweiler, Kondo, & McClusky (1981), Eckberg (1975a, 1975b), and Eckberg & Edlen (1978). Because of the extreme line blending in the UV, particularly in the Fe V–VI spectral region ($\lambda\lambda$ 1250–1700) synthetic line spectra were produced by broadening the tabulated lines with a Gaussian line profile and adding contributions from overlapping lines. This procedure allows the inclusion of broad emission lines as well as narrow photospheric absorptions. The comparison of the UV data with synthetic spectra constructed in this manner was found to be a very useful aid for the identification of the line features in the WN4-6 spectra (Koenigsberger 1990).

3. OVERVIEW OF THE SPECTRA

An overall view of HD 5980's *HST*/STIS spectra is presented in Figure 2, where we have plotted the nonereddened spectral energy distribution between $\lambda\lambda$1170 and 9000 on a log-log scale. Each plot contains the spectra at two different orbital phases. In Figure 2*a* we illustrate the spectra at $\phi = 0.83$ (near elongation when star A is approaching the observer) and at $\phi = 0.36$ (eclipse with star B on the near side; *dotted line*). The strong ISM lines have been truncated in this plot for clarity, and are flagged with a "T." The relative shift in the flux levels in these two spectra is due to the eclipse of star A by star B and amounts to a diminution in the continuum of $\Delta m \sim 0.2 \pm 0.1$ mag at eclipse in the wavelength range $\lambda\lambda$ 1600–6000. In Figure 2*b* we show the comparison between orbital phases 0.05 and 0.36, which discloses a very strong similarity between the flux levels in these two orbital phases, except in the wavelength range $\lambda\lambda$2140– 5000, in which the spectrum at phase 0.05 is brighter, by as much as 0.08 mag, with the peak occurring at λ 3000.

Some of the principal ionic species contributing to the emission lines are identified on these plots. The spectrum of HD 5980 contains lines from ionization stages ranging from neutral H (the Balmer series) up to Fe VI. A classification of the observed optical spectrum of HD 5980 yields discrepant results, depending on whether the classification criteria used rely on the He lines (Smith et al. 1996) or on the N lines (see Walborn & Fitzpatrick 2000). The ratio of He II 5411/He I 5876–0.75 suggests a WN7 spectral type, while the strength of He I 3888 and He I 4471 suggest a spectral type even as

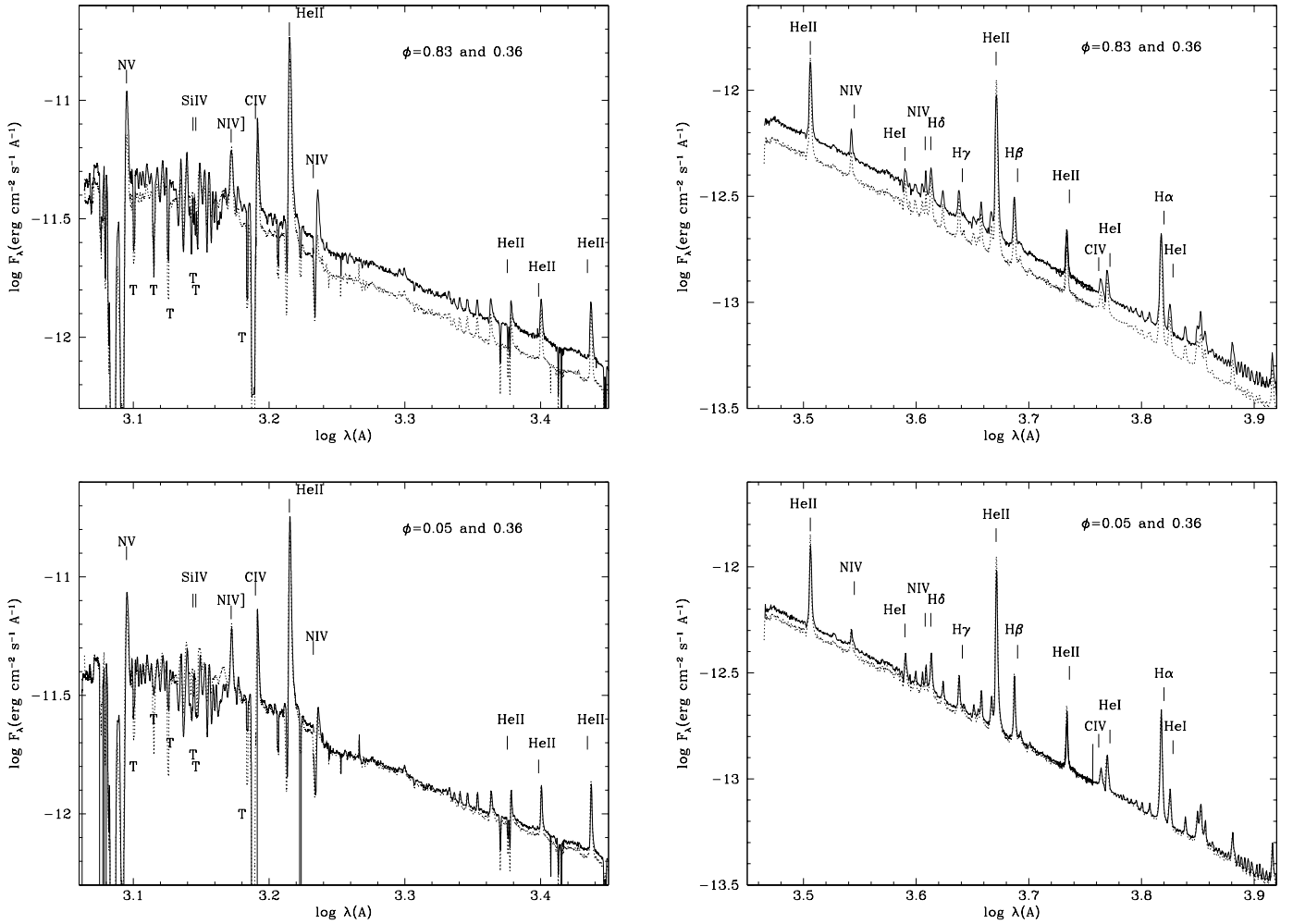

FIG. 2.—(*a*) Spectral energy distribution at orbital phases 0.83 and 0.36 (*dotted line*). Dominant contributing ionic species are identified. The strong ISM lines have been truncated for clarity in the figure, and are flagged with a "T." The difference between the continuum levels is due to the eclipse of star A by star B at $\phi = 0.36$. (*b*) Same as Fig. 2*a* for orbital phases 0.05 and 0.36 (*dotted line*).

late as WN8. However, the relative strength of N V/N III indicates a spectral type of WN5 and that of N IV/N III indicates WN5/6. Koenigsberger et al. (1996) concluded that the last UV spectra obtained with the *IUE* (in 1995) have a strong resemblance to the galactic WN 6 star HD 193077 (W-R 138), consistent with the higher temperature classification implied by the nitrogen lines. The discrepancy between the spectral types (and effective temperatures) derived from He and N diagnostics has been discussed by Crowther (1999) and Hamann (1999), who conclude that nitrogen may serve as a more sensitive diagnostic of the stellar temperature because the N IV–V lines originate from the inner wind, as opposed to He I, which is formed further out. We thus adopt WN6 for the current spectral type.

Some of the emission-line variations which occur as a function of orbital phase can be clearly observed in Figure 2*a*. The maximum intensity of N IV]1486, He II 2733, He II 3203, He II 4686, He II 5411, Hβ, and Hα does not decrease at the time of the eclipse at phase 0.36. For these lines the line-to-continuum ratio *increases* at $\phi = 0.36$ as compared to $\phi = 0.83$. However, the amount of energy contained in these lines (see Table 3) does not change significantly. A contrasting behavior is presented by the strongest lines having P Cygni absorption components (N V 1240, C IV 1550, He II 1640, N IV 1718), where the emission-line fluxes decrease by as much as factors of 2 at $\phi = 0.36$, compared with $\phi = 0.83$. These lines are more susceptible to being affected by atmospheric or wind eclipses (Khaliullin & Cherepashchuk 1976; Koenigsberger & Auer 1985; Auer & Koenigsberger 1994), where the net result is a reduction in the emission-line integrated flux and an increase in the P Cygni absorption component's strength. A third group of lines (specifically, the weaker emission lines such as Fe V, Fe VI) present a yet different type of phase-dependent variability that will be discussed below: their P Cygni absorption components disappear at phase 0.36, possibly because of the geometrical eclipse by star B of the accelerating wind regions in star A.

4. THE SPECTRUM AND RV CURVE OF STAR A

Star A is the object believed to have undergone the transition in its stellar wind structure leading up to the LBV-type eruption. This conclusion relies on the radial velocity measurements of lines that appeared as the transition was taking place (Barbá et al. 1996). Lines that were not present in the earliest *IUE* spectra, such as Si IV, N IV], Fe V, and Fe VI in the far UV (Koenigsberger et al. 1994) and N III in the optical (Barbá, et al. 1997), appeared in the 1980s and

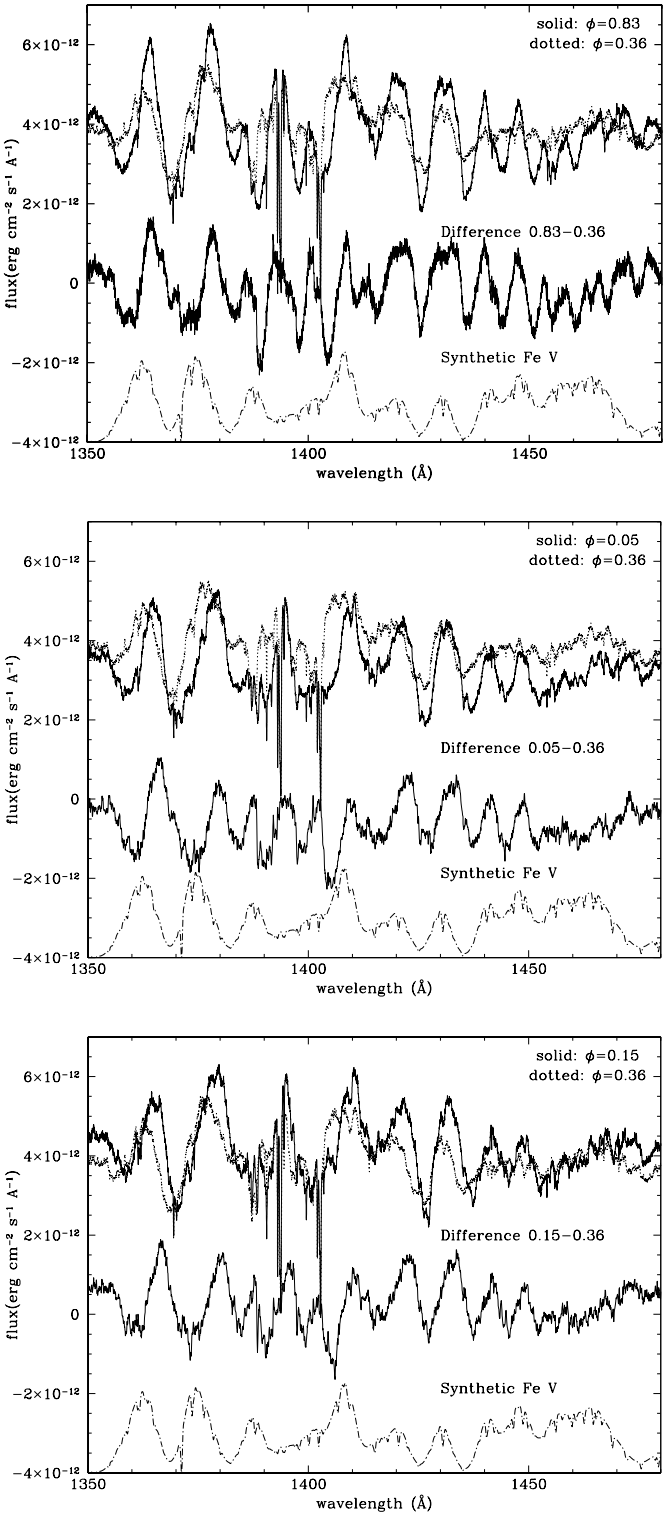

FIG. 3.—(*a*) Comparison of the spectra at $\phi = 0.83$ and 0.36 (*dotted line*) in the Si IV and Fe V spectral region illustrating the weaker or absent P Cygni absorption components at $\phi = 0.36$ (*top set of plots*); the difference between the two spectra (*middle plot*); and the synthetic Fe V spectrum (*lower plot*), which has been shifted downward for clarity. The *HST* data have been shifted in wavelength to correct for the motion of the SMC ($+150$ km s^{-1}). (*b*) Same as Fig. 3*a* but for orbital phases 0.05 and 0.36 (*dotted line*). (*c*) Same as Fig. 3*a* but for orbital phases 0.15 and 0.36 (*dotted line*).

increased in strength as the wind transition proceeded. Thus, these lines can be associated unambiguously with the wind of star A, although a possible contamination by the wind-wind collision region between the two stars cannot be discarded.

The spectral region $\lambda\lambda$ 1250–1500 contains a concentration of Fe V and Fe VI lines, as well as Si IV and scattered N IV lines. All of these lines are relatively weak, and they blend together, forming a *pseudocontinuum.* Phase-dependent line profile variations can be observed in the lines that are strong enough to rise above the pseudocontinuum and consist of a decrease in the emission and absorption components' strengths at orbital phases 0.36 and 0.40. This is illustrated in Figures 3*a*–3*c* (Fe V + Si IV) and 5*a*–4*c* (Fe VI), where each panel contains the following: the topmost portion is the plot of two spectra at different phases, unshifted in the absolute, undereddend flux coordinate, and shifted in the wavelength coordinate only to correct for the motion of the SMC ($+150$ km s^{-1}); the middle shows the difference between these two spectra; the bottom plots a synthetic Fe V (FWHM = 600 km s^{-1}) and/or Fe VI (FWHM = 300 km s^{-1}) spectrum. The Fe V lines are broader than the Fe VI lines, indicative of the ionization stratification in the stellar wind (higher degrees of ionization closer to the stellar surface), and that lines from these ions are being emitted primarily in the accelerating portion of the wind. The phase-dependent variations in the P Cygni absorption components are much more prominent in the Fe V lines than in the Fe VI lines, also implying a much more extended wind region for Fe V than for Fe VI. Figure 3*a* (phases 0.83 vs. 0.36) illustrates most clearly how the Fe V and Si IV P Cygni absorption components weaken or disappear at phases 0.36 and 0.40, when star A is eclipsed by star B. The absorptions are present at all the other orbital phases. This behavior can be interpreted as being the result of the geometrical occultation by star B of the line of sight to the continuum-emitting disk of star A, where the P Cygni absorptions arise. An alternative interpretation is that the strong radiation pressure of star B and the wind-wind collision region alters the accelerating wind structure of star A facing its companion to the extent that these P Cygni absorption components do not form. However, both interpretations rely on the formation of Fe V, Fe VI, and Si IV in the wind of star A.

The absence or weakening of the Fe V P Cygni absorption components at $\phi = 0.36$ is confirmed by a more detailed comparison between the synthetic and the observed spectra shown in Figure 4. Because the synthetic spectrum does not include any radiation transfer effects, it is a purely emission-line spectrum, and it compares most favorably with the observations at this orbital phase.

The possibility that most of the emission lines originate in the wind-wind collision region between stars A and B (see Moffat et al. 1998) has been raised. However, it is not possible to explain the presence of P Cygni absorption components at all phases other than 0.36 and 0.40 with such a scenario. The P Cygni absorption components are formed by the column of outward expanding wind material that is projected against the continuum-emitting disk of the star. If the Fe V lines were formed in a wind-wind collision shock cone wrapped around star B or in a plane perpendicular to the orbital plane, the P Cygni absorptions would have to be much weaker or absent at orbital phase 0.05, which is not the case (Figs. 3*b* and 5*b*). Thus, the conclusion that these P

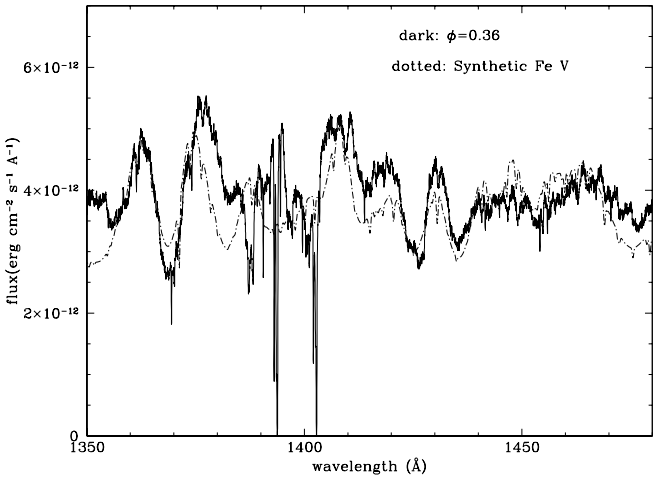

FIG. 4.—Comparison of the spectrum of HD 5980 at phase 0.36 (eclipse of star A by star B) with the synthetic Fe V spectrum, which includes both emission lines (broadened to FWHM = 600 km s^{-1}) and absorption lines (broadened to 50 km s^{-1}). The observed data have been shifted only to correct for the motion of the SMC (+150 km s^{-1}). The synthetic spectrum was scaled to fit the line at 1366 A. Note the good coincidence between the photospheric absorption features produced in star C and the synthetic Fe V absorptions.

Cygni lines are associated with the expanding wind of star A seems to be unavoidable.

Given that the Fe V and Fe VI lines arise mostly, if not completely, in star A, we can argue that lines from these ions, provide the most reliable means for measuring the orbital motion of this star, particularly because they are formed in the inner portions of the wind and are thus less prone to the interaction effects in the system. In Figure 6*a* and 6*b* we plot the radial velocity of the Fe V + VI emission blends at 1267 and 1297 Å, measured on our *HST* spectra and on the *IUE* high-dispersion spectra listed in Table 4. The *IUE* data correspond to the years 1989, 1991, and 1995. The radial velocity curve superposed on the data is based on Niemela et al.'s (1997) solution of the N V 4603 emission-line RV curve for spectra obtained in 1980–1983, but using the values of $e = 0.324$ and $\omega = 133$ given by Breysacher & Perrier (1991). The fair agreement between this RV curve and the *HST* data support the conclusion that the mass of star A is $\sim 50\ M_{\odot}$. A similar trend in the RV variations is absent in He II and C IV, consistent with these lines arising in both stars. The N IV]1486 line also follows the orbital motion of star A, although this line is more susceptible to interaction effects since it is formed in a more extended wind region. Clear evidence of these interactions is seen particularly near $\phi = 0.36$ (Fig. 6*c*). The data points that lie above the RV curve near this phase suggest the presence of a "hole" in the N IV] 1486 line-emitting region in the vicinity of star A's close companion, star B, which we will discuss further below (§ 6). This "hole" lies between the observer and star A at $\phi = 0.36$, resulting in a deficiency of emission on the short-wavelength side of the line profile, with respect to the long-wavelength side, which is produced in the receding portion (with respect to the observer) of star A's wind.

5. STAR C: THE THIRD STAR IN THE SYSTEM

The STIS echelle spectra reveal the presence of photospheric absorption features, most of which remain fixed in wavelength over the five *HST* observations and whose pro-

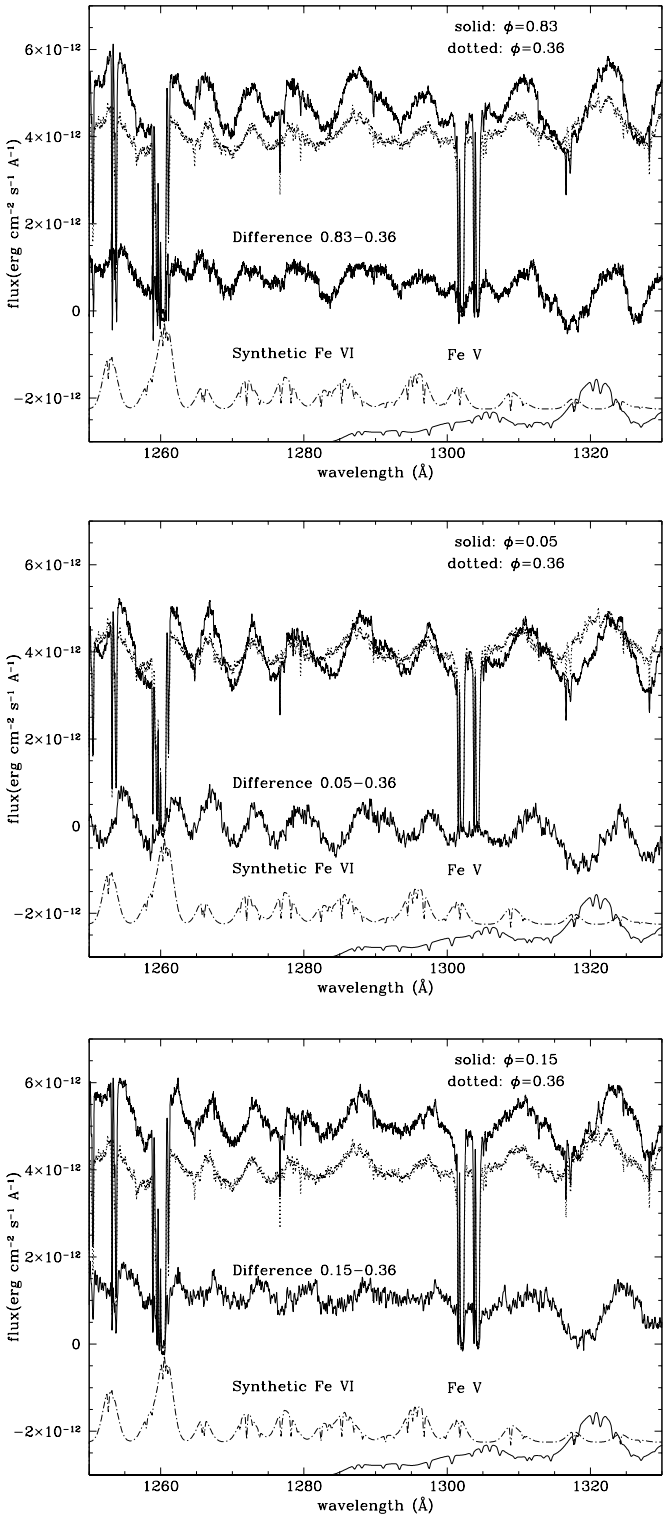

FIG. 5.—(*a*) Comparison of the spectra at $\phi = 0.83$ and 0.36 (*dotted line*) in the Fe VI spectral region illustrating the weaker P Cyg absorptions and emission lines $\phi = 0.36$ (*top set of plots*); the difference between the two spectra (*middle plot*); and the synthetic Fe VI (*dashed line*) and Fe V spectra (*lower lines*) which have been shifted downward for clarity. The *HST* data have been shifted in wavelength to correct for the motion of the SMC (+150 km s^{-1}). (*b*) Same as (*a*) for orbital phases 0.05 and 0.36 (*dotted line*). (*c*) Same as (*a*) for orbital phases 0.15 and 0.36 (*dotted line*).

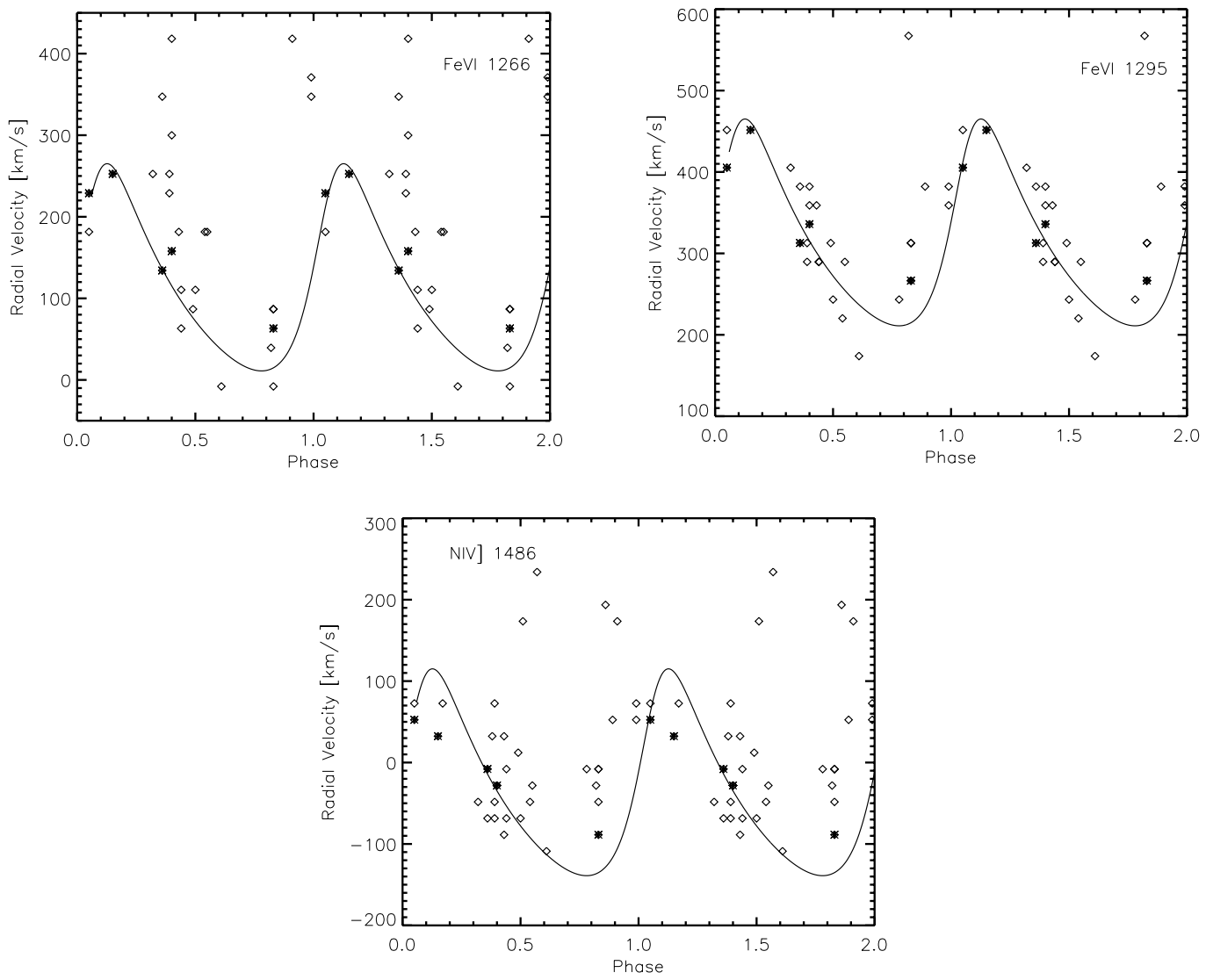

FIG. 6.—Radial velocity curve of (*a*) Fe VI 1266 A, (*b*) Fe VI 1296 A, and (*c*) N IV] 1486 emission lines measured in *IUE* spectra (*open symbols*) of 1989, 1991 and 1995 and the *HST* data (*filled symbols*). The same data are plotted twice.

files are well fitted by a Gaussian shape with FWHM = 100 km s^{-1}, on the average. Tables 5 and 6 present measurements of a selection of these absorption features present in all five of the orbital phases. These absorption lines were identified using synthetic spectra of various ions and the STIS spectra of five NGC 346 stars from the *HST* archive. The first column of these tables contains a reference wavelength; the second column presents, the identification. In Table 5 columns (3)–(7) present the individual wavelength measurements made on the spectra of HD 5980, column (8) presents the average and standard deviation of these measurements, and columns (9) presents the average and standard deviation measured in the NGC 346 stars. The listed lines observed in HD 5980 and in the NGC 346 stars coincide in wavelength to within $\sim \pm 0.2$ Å, and the wavelength position of these lines in HD 5980 remains nearly fixed over the 11 days of the observations.

In Table 6 we present the equivalent-width measurements for the five NGC 346 stars and the average equivalent width found for HD 5980. The equivalent widths are given in miliangstroms. It is important to insist upon the fact that it is very difficult to measure accurate photospheric absorption-line equivalent widths in the spectrum of HD 5980 because, with the possible exception of O IV 1338 Å, all the lines lie on top or on the wings of broad emission lines, and it is most likely that only the core of the line is being measured. Hence, these equivalent widths should just be used as indicative of the presence and relative strength of these features. Also, in order to compare the EWs in HD 5980 with those of other stars, they must be corrected for the presence of the close binary pair, (stars A + B).

Figures 7*a*–7*c* illustrate the photospheric lines in HD 5980 and in two of the NGC 346 stars, [NGC 346-355, O3V((f+)), and NGC 346-113, O6V] shown for comparison. The identifying numbers in these stars correspond to the numbers given by Massey et al. (1989). Also plotted in these figures are synthetic spectra of Fe V, Fe VI, O IV, and O V lines, taken from the line lists, and broadened with a Gaussian profile to FWHM = 100 km s^{-1}. There is no question about the reality of the Fe V and O IV photospheric absorptions in HD 5980. However, we are not able to detect lines that can be associated unambiguously with

TABLE 4

LONG-TERM TRENDS IN THE DATA OF HD 5980

		C IV 1550		He II 1640		N IV] 1486		1338	1267	1298
Spectrum	ϕ	RV	Flux	RV	Flux	RV	flux	RV	RV	RV
4277	0.57	1050	18.6	510	41.4	380	1.1	30	380	...
4345	0.91	930	17.3	460	42.6	320	1.2	−20	210	...
4958	0.68	950	19.4	440	38.9	...	0.0	50	...	...
11175	0.48	1050	16.6	400	41.9	...	0.0	70	...	...
11190	0.60	950	21.6	490	55.9	...	0.0	40	...	...
15072	0.80	910	18.6	400	65.7	...	0.0	−2	...	...
15080	0.85	1010	21.6	350	54.1	...	0.0	0	...	...
37759	0.39	890	16.4	25	67.6	100	14.5	...30	20	−70
37568	0.44	990	19.4	310	71.1	81.5	15.8	−10	−140	−70
37781	0.55	970	24.2	350	84.6	120	14.8	−30	−20	−70
37788	0.61	910	25.0	330	91.1	41.1	14.2	−20	−210	−180
42446	0.83	890	29.1	310	103.3	100	14.4	10	−120	−50
42470	0.05	990	21.7	420	74.9	220	15.3	10	−20	90
42694	0.39	810	17.5	270	67.0	80	13.7	−30	50	−50
42702	0.44	830	17.7	290	69.6	140	12.1	−20	−90	−70
42711	0.49	910	21.9	350	81.8	160	15.3	−20	−120	−50
42721	0.54	870	22.9	350	87.4	100	14.5	20	−20	−140
52888	0.51	...	0.0	...	0.0	323.4	6.9	−10	...	...
53036	0.39	830	9.6	72.2	19.7	220	13.7	10	...	...
53129	0.86	850	9.0	350	21.3	340	7.9	10	...	...
53185	0.17	810	7.6	440	20.6	220	9.9	20	...	...
53216	0.38	910	13.8	510	47.5	180	23.3	−40	...	...
53226	0.43	890	15.7	490	56.4	60	20.5	−30	...	...
54064	0.89	780	27.8	380	85.9	200	34.2	0	...	20
54490	0.32	780	25.2	310	85.5	100	40.6	−60	50	50
54671	0.36	740	30.0	310	84.5	80	36.6	−20	140	20
54727	0.82	780	34.7	420	102.0	120	27.0	...	−160	210
55315	0.78	780	39.3	360	117.3	140	35.1	−10	...	−120
55380	0.40	720	29.4	270	94.0	120	40.0	−90	210	20
55394	0.50	810	31.7	310	102.1	80	35.1	...	−90	−120
55932	0.83	810	39.4	350	123.9	140	34.6	−10	−120	−90
55955	0.99	810	34.1	400	92.5	220	32.7	−20	170	0
56017	0.40	800	27.6	290	83.7	120	35.4	−10	90	0
56188	0.83	870	38.0	290	120.2	140	27.2	...	−210	−50
56205	0.99	850	33.5	330	102.4	200	26.8	10	140	20
56223	0.43	830	25.0	310	84.7	180	26.5	40	−20	0
o1070	0.83	870	34.3	310	133.4	60	18.4	60	−140	−90
o3070	0.05	930	28.1	360	106.0	200	22.5	70	20	50
o4070	0.15	950	37.4	440	124.3	180	24.7	40	50	90
o5070	0.36	800	25.1	290	98.6	140	22.4	50	−70	−50
o6070	0.40	830	25.4	310	104.0	120	23.9	50	−50	−20

NOTE—Velocities are the centroid of the line, in km s^{-1}, corrected for the SMC motion. fluxes are not corrected for reddening and are in units of 10^{-12} ergs cm^{-2} s^{-1}.

Fe VI lines (note the Fe VI lines at $\lambda\lambda$1271.5 and 1285.5, marked with an asterisk over the plot of the O3 star in Figure 7*c*, but absent in the later subtypes and in HD 5980). We also note that the C III λ1248 line is very weak in the O3 and O4 stars, becoming stronger for later subtypes, and is relatively strong in HD 5980.

The strong Fe V lines, the present C III 1247, and the absent or very weak Fe VI and Si III λ1299 imply a spectral type for star C between O4–O7. The luminosity class can be constrained by the fact that star C contributed $\sim$30% of the optical luminosity of the system in the late 1970s (Breysacher & Perrier 1980). Given the early spectral subtype, we expect a similar contribution in the far UV wavelength range. A single main-sequence star cannot fulfill this luminosity requirement, as a comparison of the NGC 346 O4V star's continuum and that of HD 5980 in 1979 immediately illustrates: At 1500 Å, the continuum of HD 5980 is 6.5 times brighter than that of NGC 346–324. On the other hand, a supergiant such as the O7If star Sk 80, which lies close to HD 5980 in the SMC, satisfies the luminosity constraint (HD 5980 is only 2.2 times brighter than Sk 80 at 1500 Å), but Sk 80 has strong P Cygni profiles at Si IV λ1400. All supergiants cooler than O4 have significant P Cygni profiles in Si IV λ1400 (Walborn & Nichols-Bohlin 1985), and thus these features would have been visible in the spectra of HD 5980 obtained in 1979 with *IUE*. At least one spectrum (SWP 4345) reveals a weak Si IV P Cygni absorption component with maximum velocity of 1500 km s^{-1}, but this feature is not as prominent as would be expected from a O6–7 supergiant companion. We thus conclude that star C is most likely either a O4–5 supergiant or a multiple system itself, containing O4–7 main-sequence stars and/or giants. The fact that the C IV λ1500 P Cygni absorption components are saturated suggests that star C has such a

TABLE 5

WAVELENGTHS OF PHOTOSPHERIC ABSORPTIONS

		SPECTRUM						
λ_{ref} (1)	ID (2)	o1070 (3)	o3070 (4)	o4070 (5)	o5070 (6)	o6070 (7)	HD 5980 (Average ± s.d.) (8)	NGC 346 (Average ± s.d.) (9)
1248.....	C III47.38	48.08	48.13	48.06	48.15	48.16	48.12 ± 0.04	48.32 ± 0.14
1277.....	C I(ism)	77.83	77.84	77.87	77.86	77.89	77.86 ± 0.02	77.75 ± 0.06
1287.....	Fe v87.10	87.98	87.84	87.96	87.97	87.91	87.93 ± 0.06	87.74 ± 0.36
1308.....	Fe v07.42	7.81	8.25:	9.26	8.38	8.02	8.34 ± 0.56	8.30 ± 0.11
1322.....	...	22.20	22.29	22.17	22.21	22.22	22.22 ± 0.04	22.27 ± 0.09
1339.....	O IV38.61	39.55	39.51	39.42	39.51	39.54	39.51 ± 0.05	39.51 ± 0.14
1344.....	O IV43.51	44.10	44.11	44.16	44.09	44.07	44.11 ± 0.03	44.26 ± 0.11
1362.....	Fe v bl	62.24:	62.31	62.44	62.40	62.29	62.34 ± 0.08	62.52 ± 0.11
1372.....	Fe v bl	72.18	71.88	72.58	72.69	71.83	72.23 ± 0.39	72.27 ± 0.35
1374.....	Fe v bl	74.60	74.25	73.98	74.64	74.54	74.40 ± 0.28	74.61 ± 0.14
1377.....	Fe v bl	77.26	77.26	77.44	77.39	77.32	77.33 ± 0.08	77.26 ± 0.11
1407.....	O IV07.39	7.94:	7.35:	6.89	7.70	7.62	7.50 ± 0.40	7.75 ± 0.12
1410.....	Fe v bl	10.65	10.44	10.25	10.22	10.28	10.37 ± 0.18	10.18 ± 0.14
1431.....	Fe v30.57	31.72	31.54	31.38	31.56	31.46	31.53 ± 0.13	31.51 ± 0.14
1441.....	Fe v bl	41.92	41.71	41.56	41.51	41.66	41.67 ± 0.16	41.67 ± 0.11
1447.....	Fe v bl	46.96	45.45	46.24	47.48	em?	46.53 ± 0.88	47.49 ± 0.14
1449.....	Fe v48.85	49.64	49.84	49.84	49.80	49.73	49.77 ± 0.09	49.64 ± 0.10
1502.....	S V01.80	2.60	2.69	2.53	2.72	2.67	2.64 ± 0.08	2.68 ± 0.13
1624.....	Fe IV bl	...	24.50	24.59	24.67	24.78	24.63 ± 0.12	24.57 ± 0.09

saturated absorption component, making us favor an O4I classification or a multiple system containing two early-type giants.

We must, however, note a problem with the wind terminal velocities: O4I stars have $V_\infty \sim 2800$ km s^{-1}, but we do not see a persistent velocity of this magnitude in HD 5980 (the velocity that is stable throughout all the UV observations available is $\sim$1750 km s^{-1}; Koenigsberger et al. 1998a). On the other hand, the stars in the SMC are supposed to have slower wind velocities (Walborn et al. 1995) than their galactic counterparts, suggesting a solution to this apparent contradiction.

6. ORBITAL PHASE-DEPENDENT LINE PROFILE VARIATIONS

The emission-line profiles in the spectra of HD 5980 undergo very strong phase-dependent variability on the orbital timescale. In § 4 we described how the P Cygni absorption components of Fe v, Si IV lines become significantly weaker at orbital phase 0.36, when star A is eclipsed by star B. A much more prominent type of variability suffered by other, stronger lines is the diminution in their FWHM at the time of the eclipses. In the optical line of He II 4686, these variations have been observed since 1955

TABLE 6

EQUIVALENT WIDTHS OF PHOTOSPHERIC ABSORPTIONS

λ_{ref}	Ion	n355 O3V	n324 O4V	n368 O5.5V	n113 O6V	n12 O9.5V	HD 5980 (average ± s.d.)
1248.....	C III	15.	17.	84.	131.	207.	50 ± 25
1279.....	Fe VI	211.	72.	45.	15.	43.	...
1283.....	Fe VI	147.	57.	78.	39.	np?	...
1287.....	Fe v	130.	85.	61.	57.	102.	21 ± 7
1308.....	Fe v	44.	56.	68.	61.	31.	37 ± 13
1322.....	Fe v	99.	126.	174.	101.	np	30 ± 11
1338.....	O IV	448.	395.	343.	248.	143.	70 ± 19
1344.....	O IV	666.	599.	567.	379.	183.	223 ± 36
1362.....	Fe v bl	310.	316.	404.	130.	134.	71 ± 36
1363.....	Fe v bl	278.	197.	254.	229.	58.	44: ± 8:
1372.....	Fe v bl	np	633.	527.	115.	95.	118 ± 76
1374.....	Fe v bl	227.	850.	459.	146.	31.	124 ± 71
1377.....	Fe v bl	230.	255.	286.	160.	95.	72 ± 22
1407.....	O IV	376.	378.	534.	223.	59.	74 ± 39
1410.....	Fe v bl	443.	446.	613.	343.	90.	74 ± 18
1431.....	Fe v	288.	319.	330.	218.	107.	62 ± 22
1441.....	Fe v bl	362.	354.	447.	118.	113.	50 ± 22
1447.....	Fe v bl	276.	199.	218.	95.	98.	51 ± 28
1449.....	Fe v bl	296.	268.	338.	68.	60.	44 ± 11
1502.....	S V	308.	322.	344.	196.	181.	106 ± 25
1624.....	Fe IV bl	36.	46.	28.	130	153	61 ± 16

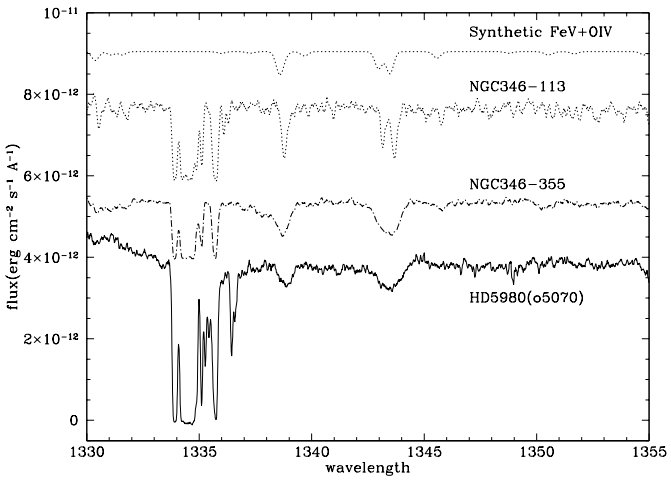

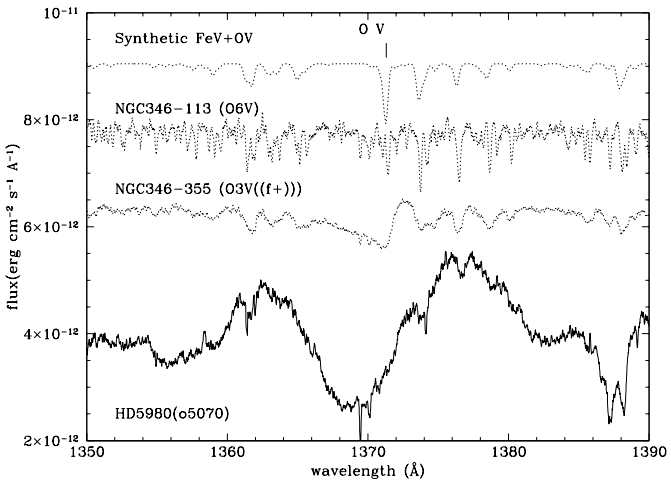

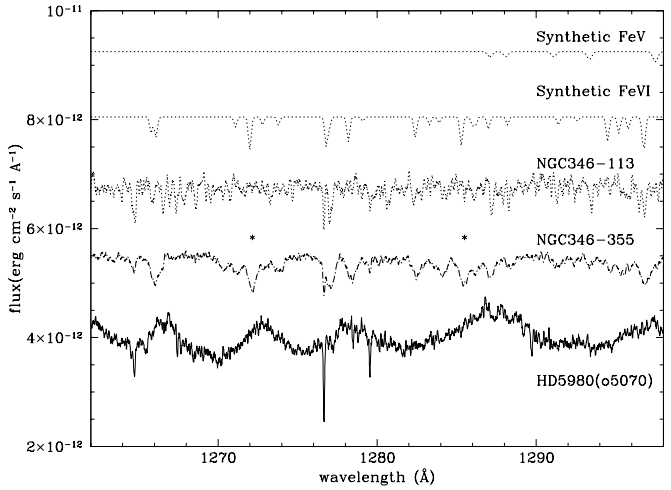

FIG. 7.—Photospheric absorption lines in the spectrum of HD 5980, belonging to star C compared with the spectra of two MS stars in NGC 345 and with synthetic spectra constructed with Fe V, Fe VI, O IV and O V lines. The blend of lines of C II λ1335 is produced by the ISM systems of the Galaxy and the SMC. The asterisks in panel (*c*) indicate lines of Fe VI present in the O3 star but absent in the O6 star and in HD 5980. The sharp line at 1277 Å is due to the ISM line of C I.

(Feast, Thackeray, Wesselink 1960; Breysacher, et al. 1982), and they are evident in the UV lines as well (Moffat, Koenigsberger, & Auer 1989). In Figure 8 we display the N IV] 1486 line profiles in the *HST* spectra, illustrating this type

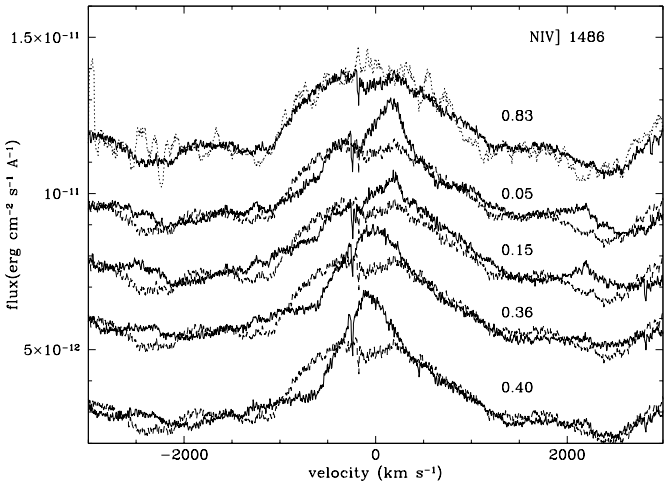

FIG. 8.—Montage of the N IV] 1486 line profiles in HD 5980. The $\phi = 0.83$ profile is compared with the same line in the Galactic WN6 star HD 193077 (W-R 138; *dotted line*), which was scaled to match that of HD 5980 by multiplying it by a factor of 1.6. The remaining profiles of HD 5980 are compared with the $\phi = 0.83$ profile (*dashed lines*), each having been corrected in the velocity scale for the SMC motion and for the orbital motion of star A. The vertical shift of the spectra is arbitrary, to ensure clarity of the figure.

of variability with a line that can be associated exclusively with the LBV-type variable star component in the HD 5980 system (i.e., star A). We believe this to be the only strong line that can be unambiguously associated with star A because the other strong lines were present to some extent in the late 1970s, and thus we assume they include a contribution from star B, and possibly star C (for example, C IV 1550 and N V 1240). However, N IV] 1486 was absent at that time. In Figure 8 we have shifted the line profile on the velocity axis to correct for the relative motion of the SMC and for the orbital motion of star A, using the relative shift implied by the Fe V/VI RV curve (Figs. 6*a*–6*b*).

In Figure 8 we also plot (superposed only on the $\phi = 0.83$ spectrum) the scaled N IV]1486 profile that is observed in the Galactic WN6 system HD 193077 (=WR 138, van der Hucht et al. 1981). Koenigsberger et al. (1996) showed that the UV spectra of HD 5980 in its current state of activity and HD 193077 are extremely similar. HD 193077 is a very long period ($\sim$1538 days) binary system (Annuk 1990) in which only very weak interaction effects in the optical and UV spectra might be expected, and in which no significant UV line-profile variability was detected (Koenigsberger & Auer 1984). Thus, the line profiles in WR 138 may be assumed to be formed in the relatively unperturbed stellar wind of the WN6 star of the system, and may be used as a template for understanding the line profile changes in HD 5980. The line profiles in HD 5980 that most resemble those of HD 193077 occur at orbital phase 0.83. This leads us to conclude that the line profiles in HD 5980 that are observed at orbital phase 0.83 are the least distorted profiles. Hence, the deformations observed at the other phases must be interpreted as the result of a departure from spherical symmetry in the line-emitting region of HD 5980 combined with eclipse effects. Whether the wind is less distorted by the interaction effects at phase 0.83 or whether the distortion of the line emitting region is simply not visible to us at this orbital phase (affecting mostly the emission-line center, for example) cannot be determined at this time, without modeling the line profiles in detail.

One scenario that predicts a departure from spherical symmetry is a wind-wind collision shock cone, which would produce a "hole" in the extended N IV]-emitting region of star A (extending beyond the orbital separation). At $\phi = 0.36$, the shock cone is pointing towards the observer reducing the amount of line emission from the outward-moving wind in the direction of the observer. This scenario is supported by the comparison of the line profiles at phase 0.36 and 0.83 (Fig. 8), where the red wings of the lines are not significantly different, while the wing at approaching velocities shows a deficiency in emission. At orbital phase 0.05, star A is between the observer and star B, and an atmospheric (or wind) eclipse occurs, reducing the emission-line intensity on both the blue and the red wings. Willis et al. (1979) detected profile variations in the C III] 1909 line in γ^2 Vel, which were attributed to a similar wind eclipse. As an alternative to the above interpretation, one could postulate that the observed emission line arises in a wind-wind collision zone lying on a plane perpendicular to the axis joining the two stars. This configuration would be expected to produce line profile variations similar (at least qualitatively) to those observed in Figure 8 (Moffat et al. 1998). However, the very strong similarity between the N IV] profiles in HD 5980 at phase 0.83 and HD 193077 would then imply that both systems have wind-wind shock regions that are very similar, both in geometrical shape and line-emitting characteristics. This seems unlikely since the orbital separation in WR 138 is so much larger than that of HD 5980.

Further support for the presence of a shock cone wrapped tightly around star B comes from the variations in the P Cygni absorption components of C IV 1550, He II 1640, and N V 1240. These lines present an increase in the extension of the absorption edges at phase 0.36, as illustrated in Figure 9. In C IV (Fig. 9*a*), the velocities go from -2500 km s^{-1} at $\phi = 0.83$ to -3300 km s^{-1} at $\phi = 0.36$; in He II (Fig. 9*b*) the corresponding velocities are -2000 km s^{-1} and -2680 km s^{-1}, respectively. These velocities are corrected for the motion of the SMC. The very high velocities are present during an extremely short time interval, since by $\phi = 0.40$ the extension of the absorption edge is nearly the same as at other orbital phases. One interpretation of these extended absorption wings is that they are the P Cygni absorption component produced in the wind of star B, and that the short duration of their visibility is due to the wind-wind shock cone winding tightly around star B with a very small opening angle. This scenario is consistent with the one given above for the N IV] 1486 line profile variations and may also explain the current lack of spectral signatures from star B at other orbital phases, since its wind is being crushed over most of its surface by the wind of star A.

The C IV 1550 line profiles of Figure 9*a* can be used to derive an estimate of the relative continuum luminosity of star C. The P Cygni absorption-line profile has a "black" region ($V_{\rm blk}$, where the flux goes to zero) that extends to a velocity of -1750 km s^{-1} in all the spectra. Within this velocity range, the three stars contribute with their saturated P Cygni absorption components, and no continuum radiation emerges. At larger velocities, there is only the contribution from stars A and B, and continuum from star C is able to reach the observer. Hence, the "plateau" that starts at -2000 km s^{-1} most likely marks the continuum level of star C. Thus, $F_{\rm starc} = 1.03 \times 10^{-12}$ ergs cm^{-1} s^{-1} Å^{-1}. This

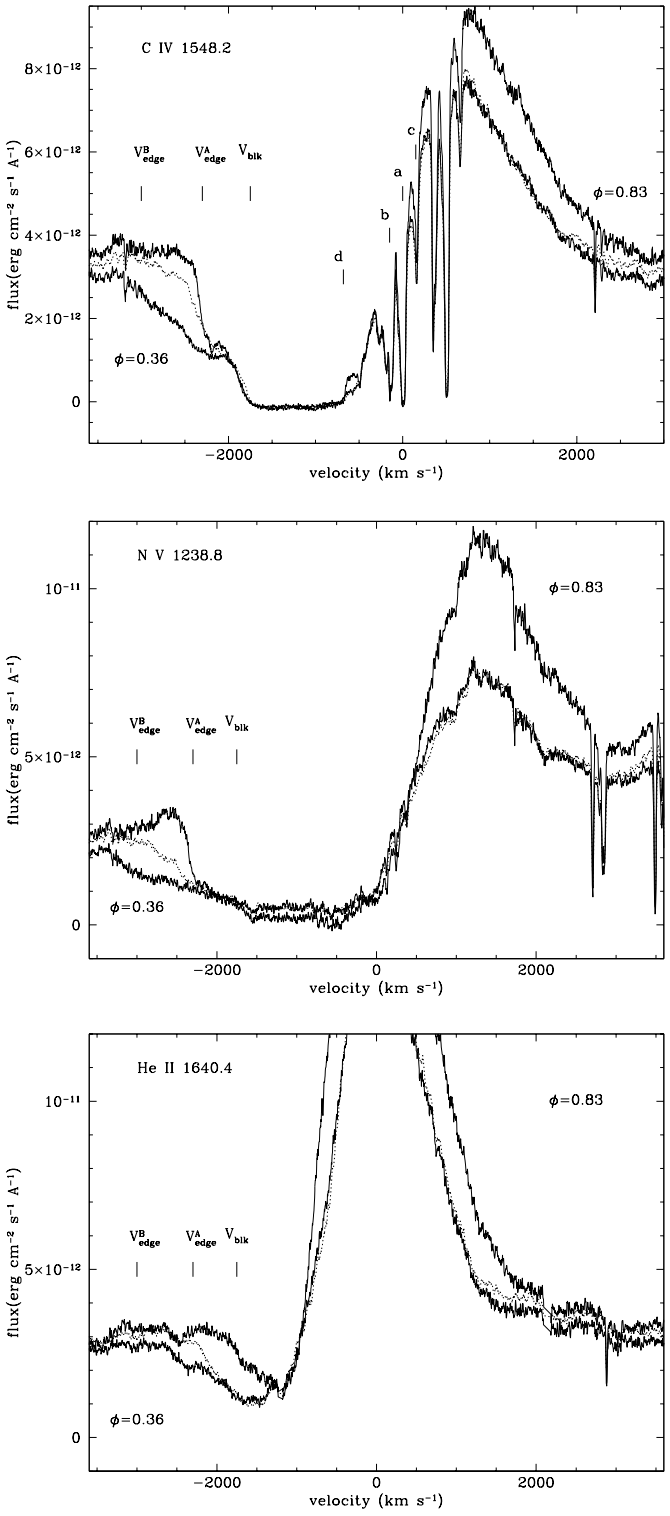

FIG. 9.—Comparison of P Cygni absorption edge velocities in (*a*) C IV 1548, (*b*) N V 1238, and (*c*) He II 1640 at three different orbital phases: $\phi = 0.36$ (*solid dark line*); 0.40 (*dotted line*); and 0.83 (*light line*). The extended absorption at $\phi = 0.36$ is interpreted as belonging to the wind of star B, constrained within a narrow wind-wind shock cone. Velocities are corrected only for the motion of the SMC. No relative shifts in the flux coordinate have been introduced. The location of the edge velocities that we tentatively associate with stars A and B is indicated on each panel of this figure; $V_{\rm blk}$ is the maximum extent of the saturated portion of the C IV absorption component. The labels a, b, c, and d in Fig. 9*a* mark the position of the four ISM components of C IV λ1548 (see § 7).

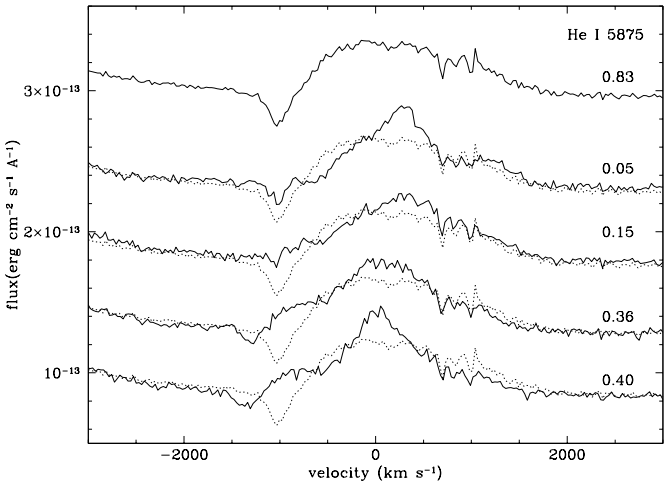

FIG. 10.—Line profiles of He I 5875 plotted as a function of velocity, corrected for the velocity of the SMC, and compared with the profile at $\phi = 0.83$ (*superimposed dotted lines*). The spectra are shifted on the vertical scale by arbitrary amounts in order to ensure clarity in the figure, and to match the continuum levels.

conclusion relies on the assumption that the C IV 1550 P Cyg absorption components in both star A and star B are saturated. This is a relatively robust assumption given the published observations of Galactic early-type stars (Walborn et al. 1985). There is, however, some uncertainty when dealing with SMC stars (Walborn et al. 1995). This value for $F_{\rm starc}$ is consistent with the $F_{\rm starc} = 1.13 \times 10^{-12}$ ergs cm^{-1}s^{-1}Å^{-1} derived from the Si IV 1393 P Cygni absorption in the *IUE* spectrum SWP 52888 (see Koenigsberger et al. 1996) if we assume that during the eruption both stars A and B were engulfed by the mass lost from star A and that this absorption component goes to zero flux intensity in both stars A and B at this time. The total continuum flux outside eclipse in the *HST* spectra is $F_{\rm A+B+C} = 3.22 \times 10^{-12}$ ergs cm^{-1} s^{-1} Å^{-1}, which yields a relative luminosity of star C with respect to the total luminosity of 32%. This is nearly the same value that Breysacher & Perrier (1980) derived for the third light source in the HD 5980 system, but for the visual wavelength region.

As a final example of the line profile variability, we present the He I 5875 line profiles in Figure 10, which display qualitative variations similar to N IV] 1486. The profile has a strong P Cygni absorption component at phases 0.83, 0.36, and 0.40; at phases 0.05 and 0.15 this absorption component has nearly vanished. There is a velocity shift between the position of the center of this absorption at phase 0.83 (~ -1000 km s^{-1}) and at phase 0.36 (~ -1250 km s^{-1}). Marchenko et al. (1994) present line profile variability in the WN5+O6 system V444 Cyg that is reminiscent of the variations present in this line in HD 5980, and which they attribute to the wind-wind collision shock cone region.

7. THE FAST-WIND/SLOW-WIND INTERACTION ZONE

The spectrum of HD 5980 contains a wealth of narrow absorption lines due to the intervening ISM. De Boer & Savage (1980) included HD 5980 in their study of the ISM components in the direction of the SMC and detected, in addition to the Galactic (at $\sim$0. km s^{-1}) and the SMC components (at $\sim +150$ km s^{-1}), components shifted to $+300$ km s^{-1} with respect to the Galactic ones. These three ISM components are illustrated in Figure 11, where we plot both lines of the Si IV doublet on a velocity scale, corrected for the SMC motion. New ISM components at -680 km s^{-1} not present prior to the LBV-type eruption are evident in this figure. We attribute these absorption components to the fast-wind/slow-wind interaction region that must have formed shortly after the velocity increase of star A's wind at the end of 1994. It is interesting to note that Koenigsberger et al. (1996) reported a similar feature at ~ -860 km s^{-1} in 1995 data (HDJ 2449930.8) and that Barbá et al. (1997) reported two narrow emission components superimposed on the He I and H I lines, at velocities ± 550 km s^{-1}, shortly after the 1994 eruption. These features, too, could be associated with the slow-fast wind interaction zone.

The velocity of the working surface (V_s) that is formed between the fast and slow winds can be used to make a crude estimate of the current mass-loss rate in HD 5980 using the relation given by Volk & Kwok (1985), under a two-wind approximation:

$$V_s^3 \frac{\dot{M}}{V} - V_s^2 \times 2\dot{M} + V_s \dot{M} V = \frac{1}{3}\, \dot{m} v^2 \ . \qquad (1)$$

Here the capital symbols stand for the slow wind values, while the lower case symbols represent the fast wind stages. Near maximum of the eruption, the wind velocities are estimated to have been ~ 300 km s^{-1}, and $\dot{M} = 10^{-3}\, M_\odot {\rm yr}^{-1}$. The current terminal velocities in the wind of star A are most likely $v \sim 2000$ km s^{-1}. Adopting $V_s = 680$ km s^{-1} the above relation yields $\dot{m} = 2 \times 10^{-4}\, M_\odot {\rm yr}^{-1}$ for the current mass-loss rate.

Clearly, this is a very rough estimate since the wind velocities have undergone systematic variations, rather than a jump from slow to fast values. In addition, the morphology of the mass-shedding event is not yet understood because the presence of the close binary companion could induce nonspherically symmetric mass loss, including, for example, the formation of a circumbinary disklike structure.

8. DISCUSSION AND CONCLUSIONS

We have presented results of the analysis of *HST* STIS observations of the brightest object in the SMC, HD 5980.

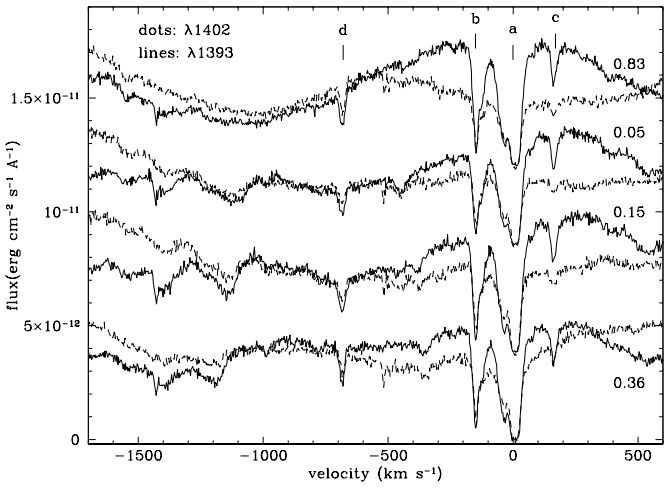

FIG. 11.—Montage of Si IV lines illustrating the previously known ISM components (a–c) and the new one at -680 km s^{-1} (d). There is no relative shift in the flux levels of corresponding λ1393 and λ1402 lines.

We confirm the existence of a third object in the system, through the detection of narrow (100 km s^{-1} FWHM) photospheric absorption lines of Fe V, C III and O IV, among others, which do not undergo significant radial velocity variations as a function of orbital phase in the 19.3 day binary system. This third object currently contributes roughly one-third of the total luminosity in the far UV wavelength region, and we suggest a spectral classification in the range of O4 to O6. If star C is a single object, its very high luminosity and lack of strong Si IV P Cygni features suggest the classification of O4I.

We argue that the Fe V/VI and N IV]1486 emission lines are the most reliable lines for measuring the radial velocity of star A, the LBV-type eruptor in the system. We find a RV curve that is consistent with that derived by Niemela et al. (1997) for this star, and thus, consistent with their derived masses for the A+B binary pair: $M_A \sim 50 M_\odot$ and $M_B \sim 28\, M_\odot$.

We conclude that the wind of star A is still dominating the hydrodynamics in the vicinity of star B, constraining the wind of star B within a narrow shock cone. Star B's wind is visible only very close to the eclipse when it is "in front" (phase 0.36). The very large wind velocity ($\sim$3000 km s^{-1}) observed only at this orbital phase in our *HST* data is similar to velocities observed in the late 1970's. There are two alternatives for this large velocity: star B has an extremely fast wind or the wind of star A is intrinsically nonspherically symmetric, with larger velocities in the direction of the companion. The first alternative has two implications: (1) star B's wind is much faster than expected for even a galactic WN4 star, being more in line with a WN2 star (see Table 2 in Hamann & Koesterke 1998), and (2) a narrow shock cone around star B was already present in 1989, constraining its wind, since the fastest edge velocity present at that time is $\sim$2200 km s^{-1}, even at $\phi = 0.39$. The second alternative implies that a mechanism is needed for producing a faster wind in the direction of star B. It is interesting to note that a spectral classification of star B as WN2 would be inconsistent with the fact that optical N V lines followed the orbital motion of star A while the N IV line followed the motion of star B, when it was visible in the spectrum (Niemela 1988), since N V would be expected to be present in the WN2 star. Hence, although we now believe that an understanding has been gained regarding the characteristics of the variable star in HD 5980, we are left with a puzzle concerning the nature of star B.

Although the transition in HD 5980 may appear to have reached a stationary state because its spectrum has not changed significantly since 1995, the trend for a continued increase in the He II 1640 Å line strength is still present. This is illustrated in Figure 12, where we plot the flux contained in the He II 1640 and C IV 1550 emission lines, as a function of Julian date, from high-dispersion *IUE* data sets and the current *HST* data set, listed in Table 4. We have excluded the data obtained close to the eruption (SWP 52888–SWP 54064) and only data corresponding to orbital phases outside eclipses ($0.50 < \phi < 0.90$) are included. It is interesting to note that the increasing trend in the emission-line strengths seems to be unaffected by the eruption. Thus, the eruption seems to have been a "transient" within a systematic change in the stellar wind properties. This "transient" could be associated with one (or several) of the following scenarios: (1) the "Ω" limit (Langer 1997) was reached, causing a large mass outflow, after which the radius of star A receded; (2) the tidal oscillations (Moreno, Georgiev, & Koenigsberger 1997) reached a critical amplitude, producing a large mass outflow, until the radius receded enough for the oscillation amplitudes to decrease; or (3) the actual eruptive event occurred in star B, in a nova-like scenario (Gallagher 1989), as a result of the accretion of star A's wind.

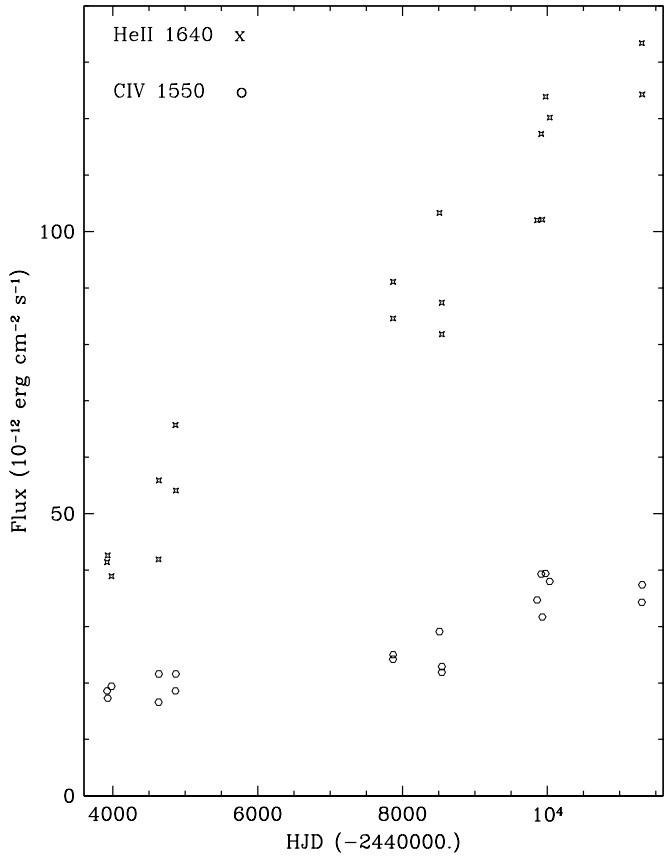

FIG. 12.—Long-term trend of the C IV1550 and He II1640 intensities showing a systematic increase over the 20 years between 1979 and 1999. Only data for phases 0.50–0.90 are plotted, and data obtained near the time of the 1994 eruption (~ HJD 49600–2449800) have been excluded.

Within all three scenarios for the eruption, the radius and the mass-loss rate of star A would be increasing systematically with time. According to the first two scenarios, the 1993 and 1994 eruptions are produced in star A, when its outer radius exceeds the maximum radius for stability within the binary system, and it undergoes an abrupt mass-shedding event, allowing it to reduce its radius and recover temporarily its stability. Multiple events such as this one would be expected to occur until the star has shed enough of its outer layers to prevent further eruptions or it reaches a new evolutionary stage. In the third scenario, the abrupt mass-shedding events of 1993 and 1994 are produced in star B, with a nova-like mechanism, as a result of the accretion onto star B of the wind emerging from star A. A significant amount of accretion is made possible by the fact that star A's wind becomes slower and denser. Clearly, however, the fact that star B is also assumed to have a strong stellar wind, which would impede accretion, makes this scenario less plausible, although we cannot discard it until the nature of star B is more clearly determined. In any case, the abrupt mass-shedding events in HD 5980 appear to be related to its binary nature, rather than to an intrinsic, subphotospheric

instability, as is believed to hold for other LBV's (Stothers & Chin 1996).

A new set of ISM components in the UV spectra of HD 5980 is detected. These components lie at a velocity of -680 km s^{-1} with respect to the SMC rest frame, and their origin is most likely in the shock interface between the slow wind ejected during the 1994 eruption and the subsequent fast wind emerging from the A+B binary system. A crude estimate using the velocity of these features and the deduced mass-loss rate in 1994 yields $\dot{m} = 2 \times 10^{-4}\, M_{\odot}\,\mathrm{yr}^{-1}$ for the current mass-loss rate.

HD 5980 has the potential of providing detailed insight into processes which take place in close binary (and probably multiple) systems, such as must be present in active sites of star formation. Its current spectral characteristics are very similar to the very massive WN stars that are being studied in the 30 Dor region R136, suggesting that some of these objects may very well be composite as is HD 5980. Furthermore, the extremely rapid (on evolutionary timescales) transition that HD 5980 has undergone demonstrates a capacity for influencing its environment on much shorter timescales than predicted from standard evolutionary models of massive stars. Starburst regions (such as R136) must contain a large number of very massive binary and multiple systems, whose evolution will influence the subsequent evolution of the stellar population within the cluster. Thus, gaining an understanding of the physical processes taking place in HD 5980 will have direct application to distant starburst regions, where similar phenomena are very likely to be occurring.

Support for this work was provided by NASA through grants GO-7480.01-96A, GO-7480.02-96A, and GO-7480.03–96A from the Space Telescope Science Institute, which is operated by AURA, Inc., under NASA contract NAS 5-26555, and from CONACYT grant 27744-E.

REFERENCES

Annuk, K. E. 1990, Acta Astron., 40, 267
Auer, R. L., & Koenigsberger, G. 1994, Apj, 466, 859
Barbá, R., Niemela, V., Baume, G., & Vazquez, R. A. 1995, ApJ, 446, L23
Barbá, R. H., Niemela, V. S., & Morrell, N. I. 1997, in ASP Conf. Ser. 120, Luminous Blue Variables: Massive Stars in Transition, ed. A. Nota & H. Lamers (San Francisco: ASP), 238
Barbá, R., et al. 1996, in Colliding Winds in Binary Stars, Rev. Mexicana Astron. Astrofis. Conf. Ser., 5, 85
Bateson, F. M., & Jones, A. F. 1994, Pub. R. Astron. Soc. New Zealand, 19, 50
Bohannan, D. 1997, in ASP Conf. Ser. 120, Luminous Blue Variable Massive Stars in Transition, ed. A Nota & H. J. G. L. M. Lamers (San Francisco: ASP), 3
Breysacher, J., Moffat, A. F. J., & Niemela, V. 1982, ApJ, 257, 116
Breysacher, J., & Perrier, C. 1980, A&A, 90, 207
———. 1991, in IAU Symp. 143, Wolf-Rayet Stars and Interrelations with other Massive Stars in Galaxies, ed. K. van der Hucht & B. Hidayat (Dordrecht: Kluwer),229
Boggess, A., et al. 1978a, Nature 275, 372
———. 1978b, Nature 275, 377
Bruhweiler, F. C., Kondo, Y., & McClusky, G. E. 1981, ApJ, 46, 255
Crowther, P. A. in IAU Symp 193, Wolf-Rayet Phenomena in Stars and Starburst Galaxies, ed. K. A., van der Hucht, G. Koenigsberger, & P. Eenens (San Francisco: ASP), 116
Crowther, P. A., & Dessart,L. 1998, MNRAS, 296, 622
Crowther, P. A., & Smith, L. J. 1996, A&A, 305, 541
de Boer, K. S., & Savage, B. D. 1980, ApJ, 238, 86
de Koter, A., Heap, S. R., & Hubeny, I. 1997, ApJ, 477, 792
Dionne, D. 1999, in IAU Symp. 193, Wolf-Rayet Phenomena in Stars and Starburst Galaxies, ed. K. A., van der Hucht, G. Koenigsberger, & P. Eenens (San Francisco: ASP), 596
Ekberg, O. 1975a, Phys. Scr., 12, 42
———. 1975b, Phys. Scr., 11, 23
Ekberg, O., & Edlen, B. 1978, Phys. Scr., 18, 107
Feast, M. W.,Thackeray, A. D., & Wesselink, A. F. 1960, MNRAS, 121, 25
Gallagher, J. S. 1997, in ASP Conf. Ser. 120, Luminous Blue Variables: Massive Stars in Transition, ed. A. Nota & H. J. G. L. M. Lamers (San Francisco: ASP), 389
Gallagher, J. S. 1989, in Physics of Luminous Blue Variables, ed. K. Davidison, A. F. J. Moffat, & H. J. G. L. M. Lamers (Dordrecht: Kluwer), 185
García-Segura, G., Maclow, M.-M., & Langer, N. 1996, A&A, 305, 229
Hamann, W.-R. 1999, in IAU Symp. 193, Wolf-Rayet Phenomena in Stars and Starburst Galaxies, ed. K. A., van der Hucht, G. Koenigsberger, & P. Eenens (San Francisco: ASP), 138
Hamman, W.-R., & Koesterke, L. 1998, A&A, 333, 251
Heap, S. 1999, in IAU Symp. 193, Wolf-Rayet Phenomena in Stars and Starburst Galaxies, ed. K. A., van der Hucht, G. Koenigsberger, & P. Eenens (San Francisco: ASP), 412
Heydari-Malayeri, M., Rauw, G., Esslinger, O., & Beuzit, J.-L. 1997, A&A, 322, 554
Hillier, J. 1995, in IAU Symp. 193, Wolf-Rayet Phenomena in Stars and Starburst Galaxies, ed. K. A., van der Hucht, G. Koenigsberger, & P. Eenens (San Francisco: ASP), 116
Humphreys, R., & Davidson, K. 1994, PASP, 106, 1025
Khaliullin, Kh., & Cherepashchuk, A. M. 1976, Soviet Astron., 20, 186
Kelly, R. L., & Palumbo, L. J. 1973, Atomic and Inic Emission Lines Below 2000 Å, NRL Report 7599
Kimble, R. A., et al. 1998, ApJ, 492, L83
Koenigsberger, G. 1990, Rev. Mexicana Astron. Astrofis. Conf. Ser. 20, 85
Koenigsberger, G., & Auer, L. H. 1985, ApJ, 297, 255
Koenigsberger, G., Auer, L. H., Georgiev, L., & Guinan, E. 1998a, ApJ, 496, 934
Koenigsberger, G., Moffat, A. F. J., St. Louis, N., Auer, L. H., Drissen, L., & Seggewiss, W. 1994, ApJ, 436, 301
Koenigsberger, G., Peña, M., Schmutz. W., & Ayala, S. 1998b, ApJ, 499, 889
Koenigsberger, G., Shore, S. S., Auer, L. H., & Guinan, E. 1996, Rev. Mexicana Astron. Astrofis. Conf. Ser., 5, 92
Langer, N. 1997, in ASP Conf. 120, Luminous Blue Variables: Massive Stars in Transition, ed. A. Nota & H. Lamers (San Francisco: ASP), 83
Langer, N., Hamann, W.-R., Lennon, M., Najarro, F., Pauldrach, A. W. A., & Puls, J. 1994, A&A, 290, 819
Leitherer, C. 1999, in IAU Symp. 193, Wolf-Rayet Phenomena in Massive Stars and Starburst Galaxies, ed. K. A. van der Hucht, G. Koenigsberger, & P. R. J. Eenens (San Francisco: ASP), 526
Maeder 1997, in ASP Conf. Ser. 120, Luminous Blue Variable Massive Stars in Transition, ed. A Nota & H. J. G. L. M. Lamers (San Francisco: ASP), 374
Marchenko, S. V., Moffat, A. F. J., & Koenigsberger, G. 1994, ApJ, 422, 810
Massey, P., Parker, J. W., & Garmany, C. D. 1989, AJ, 98, 1305
Moffat, A. F. J., Koenigsberger, G., & Auer, L. H. 1989, ApJ, 344, 734
Moffat, A. F. J., et al.. 1998, ApJ, 497, 896
Moreno, E., Georgiev, L., & Koenigsberger, G. 1997, in ASP Conf. 120, Luminous Blue Variables: Massive Stars in Transition, ed. A. Nota & H. Lamers (San Francisco: ASP), 152
Niemela, V. 1988, in Progress and Opportunities in Southern Hemisphere Optical Astronomy, ed. V. M. Blanco & M. M. Pillips (Prov: Brigham Young Univ. Press), 381
Niemela,V., Barba, R., Morrell, N., & Corti, M. 1997, in ASP Conf. 120, Luminous Blue Variables: Massive Stars in Transition, ed. A. Nota & H. Lamers (San Francisco: ASP), 152, 222
Schmutz, W. 1995, in IAU Symposium 163, Wolf-Rayet Stars: Binaries, Colliding Winds, Evolution, ed. K. A. van der Hucht, & P. M. Williams (Dordrecht: Kluwer), 127
Schmutz, W., & Drissen, L. 1999, Rev. Mexicana Astron. Astrofis. Conf. Ser. 8, 41
Smith, L. Shara, M., & Moffat, A. F. J. 1996, MNRAS, 281, 163
Sterken, C., & Breysacher, J. 1997, A&A, 328, 269
Stothers, R. B., & Chin, C. W. 1996, ApJ, 468, 842
Striganov, A. R., & Svetitskii, N. S. 1968, Tables of Spectral Lines of Neutral and Ionized Atoms (New York: IFI/Plenum)
Van Bever, J. et al. 1998, in IAU Symp. 193, Wolf-Rayet Phenomena in Stars and Starburst Galaxies, ed. K. A., van der Hucht, G. Koenigsberger, & P. Eenens (San Francisco: ASP), 624
van der Hucht, K. A., Koenigsberger, G., & Eenens, P. eds. 1999, IAU Symp. 193, Wolf-Rayet Phenomena in Stars and Starburst Galaxies, ed. K. A., van der Hucht, G. Koenigsberger, & P. Eenens (San Francisco: ASP)
Voit, M., ed. 1997, *HST* Data Handbook Vol. I

Volk, K., & Kwok, S. 1985, A&A, 153, 79
Walborn, N. R., et al. 1995, PASP, 107, 104
Walborn, N. R., & Fitzpatrick, E. L. 2000, PASP, 112, 50
Walborn, N. R., Nichols-Bohlin, J., & Panek, R. J. 1985, *International Ultraviolet Explorer* Atlas of O-Type Spectra from 1200 to 1900 A (NASA Ref. Pub. 1155)
Willis, A. J. 1999, in IAU Symp. 193, Wolf-Rayet Phenomena in Stars and Starburst Galaxies, ed. K. A., van der Hucht, G. Koenigsberger, & P. Eenens (San Francisco: ASP), 1
Willis, A., et al. 1979, in The First Year of *IUE*, ed. A. J. Willis (London: University College), 394